

AD-A187 363

AFGL-TR-87-0045

Spectral Evidence for Source Multiplicity in Explosions

Douglas R. Baumgardt
Kathleen A. Ziegler

ENSCO, Inc.
5400 Port Royal Road
Springfield, Virginia 22151 - 2388
Scientific Report No. 2

Approved for public release; distribution unlimited

AIR FORCE GEOPHYSICS LABORATORY
AIR FORCE SYSTEMS COMMAND
UNITED STATES AIR FORCE
HANSCOM AIR FORCE BASE, MASSACHUSETTS 01731

DTIC
ELECTE
NOV 23 1987
S D
H

87 11 14 050

The views and conclusions contained in this document are those of the authors and should not be interpreted as representing the official policies, either expressed or implied, of the Defense Advanced Research Projects Agency or the U.S. Government.

Semiannual Report: SAS-TR-87-01
ARPA order Number 5308
Project Title: Yield Estimation with P-Coda and Lg Measurements
Contract: F19628-85-C-0057

"This technical report has been reviewed and is approved for publication"

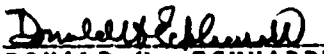


JAMES F. LEWKOWICZ
Contract Manager



HENRY A. OSSING
Branch Chief

FOR THE COMMANDER



DONALD H. ECKHARDT
Division Director

This report has been reviewed by the ESD Public Affairs Office (PA) and is releasable to the National Technical Information Service (NTIS).

Qualified requestors may obtain additional copies from the Defense Technical Information Center. All others should apply to the National Technical Information Service.

If your address has changed, or if you wish to be removed from the mailing list, or if the addressee is no longer employed by your organization, please notify AFGL/DAA, Hanscom AFB, MA 01731. This will assist us in maintaining a current mailing list.

Do not return copies of this report unless contractual obligations or notices on a specific document requires that it be returned.

REPORT DOCUMENTATION PAGE

1a. REPORT SECURITY CLASSIFICATION UNCLASSIFIED		1b. RESTRICTIVE MARKINGS	
2a. SECURITY CLASSIFICATION AUTHORITY		3. DISTRIBUTION/AVAILABILITY OF REPORT	
2b. DECLASSIFICATION/DOWNGRADING SCHEDULE		Approved for public release; distribution unlimited.	
4. PERFORMING ORGANIZATION REPORT NUMBER(S) SAS-TR-87-01		5. MONITORING ORGANIZATION REPORT NUMBER(S) AFGL-TR-87-0045	
6a. NAME OF PERFORMING ORGANIZATION ENSCO, Inc.	8b. OFFICE SYMBOL (If applicable)	7a. NAME OF MONITORING ORGANIZATION Air Force Geophysics Laboratory (LWH)	
6c. ADDRESS (City, State and ZIP Code) 5400 Port Royal Road Springfield, VA 22151-2388		7b. ADDRESS (City, State and ZIP Code) Hanscom Air Force Base Massachusetts 01731	
8a. NAME OF FUNDING/SPONSORING ORGANIZATION Defense Advanced Research Projects Agency	8b. OFFICE SYMBOL (If applicable)	9. PROCUREMENT INSTRUMENT IDENTIFICATION NUMBER F19628-85-C-0057	
8c. ADDRESS (City, State and ZIP Code) 1400 Wilson Boulevard Arlington, VA 22209		10. SOURCE OF FUNDING NOS.	
11. TITLE (Include Security Classification) Spectral Evidence for Source Multiplicity (over)		PROGRAM ELEMENT NO. 62714E	PROJECT NO. 5A10
		TASK NO. DA	WORK UNIT NO. AQ
12. PERSONAL AUTHOR(S) Douglas R. Baumgardt, Kathleen A. Ziegler			
13a. TYPE OF REPORT Scientific #2	13b. TIME COVERED FROM _____ TO _____	14. DATE OF REPORT (Yr., Mo., Day) February 1987	15. PAGE COUNT 43
16. SUPPLEMENTARY NOTATION			
17. COSATI CODES		18. SUBJECT TERMS (Continue on reverse if necessary and identify by block number)	
FIELD	GROUP	SUB. GR.	
		NORESS; mine blasts; earthquakes; ripple fire; spectral analysis.	
19. ABSTRACT. (Continue on reverse if necessary and identify by block number)			
<p>Spectral and cepstral analysis were performed on regional-array NORESS recordings of mining explosions in Scandinavia and Russia in order to detect the effects of delayed explosions or "ripple firing" commonly used in mine-blasting practice. NORESS stack spectra were computed in windows on Pn, Pg, Sn, and Lg by averaging individual channel spectra, frequency by frequency, across the array. The stack spectra were then corrected for instrument response and noise. For comparison, spectra were also computed for six western Norway earthquakes located near the Blasjo and Titania Norwegian mines. Also, stack spectra of P coda, Sn, and Lg were computed using NORSAR seismograms for presumed PNEs located at near regional distances ($\Delta = 10$ degrees) in western Russia. The NORSAR spectra were determined in the same manner as the NORESS spectra, except that an additional source correction was applied to the spectra. ←</p> <p style="text-align: center;">Delta</p>			
20. DISTRIBUTION/AVAILABILITY OF ABSTRACT UNCLASSIFIED/UNLIMITED <input type="checkbox"/> SAME AS RPT. <input checked="" type="checkbox"/> DTIC USERS <input type="checkbox"/>		21. ABSTRACT SECURITY CLASSIFICATION UNCLASSIFIED	
22a. NAME OF RESPONSIBLE INDIVIDUAL James F. Lewkowicz		22b. TELEPHONE NUMBER (Include Area Code) (617) 377-3028	22c. OFFICE SYMBOL LWH

Cont of Block 11:

in Explosions

SUMMARY

Spectral and cepstral analysis were performed on regional-array NORESS recordings of mining explosions in Scandinavia and Russia in order to detect the effects of delayed explosions or "ripple firing" commonly used in mine-blasting practice. NORESS stack spectra were computed in windows on P_n , P_g , S_n , and L_g by averaging individual channel spectra, frequency by frequency, across the array. The stack spectra were then corrected for instrument response and noise. For comparison, spectra were also computed for six western Norway earthquakes located near the Blasjo and Titania Norwegian mines. Also, stack spectra of P coda, S_n , and L_g were computed using NORSAR seismograms for presumed PNEs located at near-regional distances ($\Delta > 10$ deg.) in western Russia. The NORSAR spectra were determined in the same manner as the NORESS spectra, except that an additional source correction was applied to the spectra.

Comparison of western Norway mine-blast spectra and nearby earthquakes shows that the earthquake P_n spectra are peaked in the 3 to 16 Hz band, with little energy below 6 Hz, whereas the explosion spectra have flatter spectra from 3 to 16 Hz. This difference in the P_n spectra may be caused by the earthquakes occurring at greater depths than the explosions, differences in the near-source media, or source mechanism effects in the earthquake spectra. The main difference between earthquake and explosion spectra is that the explosion spectra exhibit marked scalloping or modulation patterns not observed in the earthquake spectra. The modulation patterns are identical in spectra of all phases, indicating that they are caused by multiple-shot sequences or ripple firing. Similar patterns have been observed in spectra of northern Sweden mine blasts and mine blasts in Russia near Leningrad. Cepstral analysis of the spectra reveals that the delay times between explosions are on the order 80 to 150 milliseconds. Moreover, the NORSAR spectra of PNEs indicate that these signals are also produced by multiple explosions, although they have larger delay times of between 0.9 to 1.5 seconds.

Simulated multiple-source spectra, determined using the NORESS seismograms for one of the western Norway earthquakes, resulted in spectra that resembled many of the explosion modulation patterns. Simulations suggest that the mine explosions, which appear to have delays on the order of hundreds of milliseconds, are composed of no more than two or three explosions that are probably of different sizes. The precise number of explosions is hard to ascertain because of the extreme complexity of cepstra produced by three or more explosions. Although it is conceivable and likely that the mine explosions have delays shorter than 50 milliseconds, the bandwidth of the data used in this study is too narrow to resolve such delays. However, spectral analysis of data from the new HFSE high-frequency element at the NORESS center should allow resolution of delays of 25 milliseconds and less.

on For	
RA&I	<input checked="" type="checkbox"/>
DTIC TAB	<input type="checkbox"/>
Unannounced	<input type="checkbox"/>
Justification	
By _____	
Distribution/	
Availability Codes	
Dist	Avail and/or Special
A-1	



INTRODUCTION

Source characterization studies of earthquakes have generally supported the view that earthquakes are not simple single point sources but rather are composites of many small ruptures caused by source heterogeneities called barriers and asperities (Papageorgiou and Aki, 1985a,b). Recent studies of large earthquakes have modelled them in terms of multiple ruptures, each one delayed by some amount of time after the initial rupture (eg, Barker and Langston, 1981, and other references therein). Small microearthquakes have less dramatic source multiplicity and directivity effects although small short-delay multiple ruptures could greatly affect the high-frequency characteristics of small-earthquakes seismograms.

Explosion sources, on the other hand, are generally thought of as being ideal point explosive sources, although many large nuclear explosions have an accompanying non-isotropic tectonic component. However, economic explosions, such as quarry and mine blasts, are known to be composed of several delayed blasts, sometimes referred to as "ripple firing". Depending on the time delays between explosions and the bandwidth of the recording seismic instruments, ripple-firing effects should be recognizable in seismic spectra and may serve as simulations of multiple ruptures in earthquakes.

If two or more explosions are fired at nearly the same location but with small time delays, the seismically recorded waveforms for each of the explosions should be very similar although their amplitudes may vary if the sizes of the delayed explosions are different. The power spectrum computed on a time window which incorporates all the delayed-explosion signals will exhibit a characteristic modulation or scalloping pattern. The amplitudes of the scallops will depend on the degree of correlation of the different signals and their relative amplitudes, and the periodicity of the scalloping will be determined by the number and length of the different time delays. Bell and Alexander (1977) computed spectrograms or sonograms of simulated multiple explosions and demonstrated that the spectral modulations would be observed throughout the entire wavetrain. This persistence of the spectral modulations in all phases of the seismograms would be a way of distinguishing multiple explosions from multipath interference, such as modulations in P spectra do to P-pP interference. Flinn et al (1973) demonstrated the application of homomorphic deconvolution, or cepstral analysis, to the detection of a simulated multiple events. However, neither of these studies applied these techniques to actual delayed seismic events.

The observability of ripple-fire effects in mine or quarry blasts could have important implications for the problem of seismic discrimination between economic explosions, small nuclear explosions and earthquakes recorded at regional distances with high-frequency seismic recorders. Past regional discrimination studies have focused on comparisons of so-called "discriminants" usually extracted from the spectra of explosions and earthquakes (Murphy and Bennett, 1982; Gupta et al, 1984, Aviles and Lee, 1986). The ultimate objective of these studies has been to find a spectral feature which reflects some intrinsic difference between explosions and earthquakes which could be used to identify the source type. However, it has proved difficult to unequivocally distinguish between spectral differences due to source and those caused by near-source geology and propagation path differences. Aviles and Lee (1986) have suggested that ripple fire effects could have been the explanation for their observation of more low-frequency energy in mine blasts compared to colocated earthquakes, although differences in near-source geology could have also produced these differences. To date, there have been no studies which explicitly show the effect of ripple fire on high-frequency spectra which could be

used to identify economic explosions.

In this study, we report on the direct observation of source multiplicity in the spectra of explosion data recorded at regional and near-regional distances. Mine blasts and earthquakes in western Norway, recorded at regional distance from the new NORESS regional seismic array, are compared which show that source multiplicity can be observed in mine-blast spectra but not in those of small earthquakes. Moreover, we also show evidence of source multiplicity in mine explosions seismograms, recorded by NORESS, in Sweden and in Russia near Leningrad as well as in presumed peaceful nuclear explosions (PNEs) in western Russia recorded at the NORSAR teleseismic array. This study will show how incoherent array-stack spectra extending to high frequency can be used for source characterization and identification of source multiplicity in explosions.

Modulated Spectra of Multiple Events

Our strategy in the detection of multiple events is to identify a spectral modulation pattern which persists in the spectra of all phases throughout the entire seismogram. It would also be desirable to discern the number and delay times of the different events. However, as we show below, this can be very difficult because scalloping patterns for multiple explosions can be very complicated, even for a small number of delays. In this section, we consider the theoretically expected spectra of seismic signals from multiple explosions, both from single and multiple delays, and discuss the delay times we expect from standard blasting practice.

Single Delay. The equation for two signals $x(t)$, delayed by time τ and scaled by α , a real value, is given by

$$y(t) = x(t) + \alpha x(t-\tau). \quad (1)$$

The Fourier transform of this signal is then

$$Y(\omega) = X(\omega)(1 + \alpha e^{-j\omega\tau})$$

giving the power spectrum

$$|Y(\omega)|^2 = |X(\omega)|^2(1 + \alpha^2 + 2\alpha\cos\omega\tau) = |X(\omega)|^2(1 + \alpha^2)\left(1 + 2\frac{\alpha}{1 + \alpha^2}\cos\omega\tau\right). \quad (2)$$

This spectrum exhibits modulations of period $\frac{1}{\tau}$ due to the $\cos\omega\tau$ term. The logarithm is now taken to "whiten" the spectrum (Kemerait and Sutton, 1982) giving

$$\text{Log } |Y(\omega)|^2 = \text{Log } [|X(\omega)|^2(1 + \alpha^2)] + \text{Log } \left(1 + 2\frac{\alpha}{1 + \alpha^2}\cos\omega\tau\right). \quad (3)$$

Using the approximation

$$\text{Log } (1+x) \approx x - \frac{x^2}{2} + \frac{x^3}{3} - \dots; \quad -1 < x \leq 1 \quad (4)$$

equation 3 can be expanded to give the following :

$$\begin{aligned} \text{Log } |Y(\omega)|^2 &= \text{Log } [|X(\omega)|^2(1 + \alpha^2)] + \beta\cos\omega\tau \\ &\quad - \frac{\beta^2}{2}\left(\frac{\cos 2\omega\tau + 1}{2}\right) + \frac{\beta^3}{3}\left(\frac{\cos 3\omega\tau + 3\cos\omega\tau}{4}\right) - \dots \end{aligned} \quad (5)$$

where $\beta = 2\frac{\alpha}{1 + \alpha^2}$. The Fourier transform of the log of the Fourier transform is defined as the cepstrum. This function exhibits spikes at τ and multiples of τ , and the magnitudes of the spikes diminish with quefreny.

Multiple Delays. A signal with N delays, with the Nth delay being scaled by α_N (a real value) and delayed by τ_N , can be described by

$$y(t) = x(t) + \alpha_1 x(t - \tau_1) + \alpha_2 x(t - \tau_2) + \dots + \alpha_N x(t - \tau_N). \quad (6)$$

The Fourier transform of this is

$$Y(\omega) = X(\omega)(1 + \alpha_1 e^{-j\omega\tau_1} + \alpha_2 e^{-j\omega\tau_2} + \dots + \alpha_N e^{-j\omega\tau_N}) \quad (7)$$

and the log power spectrum is expressed by

$$\begin{aligned} \text{Log } |Y(\omega)|^2 &= \text{Log } [|X(\omega)|^2(1+\beta)] \\ &+ \text{Log } \left[1 + \frac{2}{1+\beta} \left[\sum_{n=1}^N (\alpha_n \cos\omega\tau_n + \sum_{m=n+1}^N \alpha_n \alpha_m \cos\omega(\tau_n - \tau_m)) \right] \right] \end{aligned} \quad (8)$$

where $\beta = \sum_{n=1}^N \alpha_n^2$ is constant in τ . The approximation in equation 4 can be applied to expand equation 8 with the first term being

$$x = \frac{2}{1+\beta} \left[\sum_{n=1}^N (\alpha_n \cos\omega\tau_n + \sum_{m=n+1}^N \alpha_n \alpha_m \cos\omega(\tau_n - \tau_m)) \right] \quad (9)$$

The following terms contain increasing numbers of cosinusoidal components. The Fourier transform of equation 8 will produce peaks at the τ_n 's, the $(\tau_n - \tau_m)$'s and their harmonics, plus peaks at the quefrequencies of the higher order terms in the expansion. The amplitudes of these spikes are dependent on the amplitudes of the delayed signals (the α_n 's).

Expected Delay Times. Standard blasting practice almost always involves designing a spatial and temporal pattern which can vary depending on the application(Langefors and Kihlstrom, 1963; Dick, et al, 1983). There are three basic types of delay series commonly used (Dick et al, 1983):

- Slow or tunnel delays.
- Fast or millisecond delays.
- Coal mine delays.

Slow delays are most often used in tight blasting, such as in underground metallic or nonmetallic mines, and are designed to cause the rock burden in one blasting hole to move prior to the next detonation. Slow-delay intervals are typically on the order of 0.5 to 1.0 second. Fast delays are most commonly used under less tight conditions, such as surface blasting. The millisecond delays can be quite variable, ranging from 25 to 50 milliseconds for low-period vibrations to in excess of 100 milliseconds for longer periods. Coal-mine delays are a special series of millisecond delays used in the hazardous conditions of coal mines and are on the order of 50 to 100 milliseconds.

Dick et al (1983) give three fundamental motivations for using millisecond delays in rock blasting:

1. To assure that a proper free face is developed to enable the explosive charge to efficiently fragment and displace its burden.
2. To enhance fragmentation between adjacent holes.
3. To reduce the ground vibrations created by the blast.

The required coarseness of the fragmentation governs the length of the delays, with longer delays required for higher coarseness. For ground-vibration reduction, the required delay interval is directly proportional to the period of the strongest vibrations. Also, greater time delays

are used for larger explosives.

Another factor which must be considered in blasting is the geometric arrangement and number of blasts in a sequence. These factors vary depending on the requirements of the given blasting situation. Moreover, a blast sequence can be composed of more than one delay time or a complex combination of different delay times.

Thus, it is hard to predict what kinds of delays to expect in mine or quarry blasting because they can vary depending on the application. The shortness of delays that can be detected with spectral analysis is determined by the bandwidth of the recording system. However, equations 8 and 9 show that the various periodicities in the spectral modulations depend not only on the basic delay, τ_n , but also the interaction of delays, $\tau_n - \tau_m$. If there are many delays of different lengths, then the resulting spectrum in equation 8 can be very complex.

DATA AND ANALYSIS PROCEDURES

NORESS and NORSAR Data. The data used for this study were recorded at the NORESS and NORSAR arrays both located about 100 km north-northeast of Oslo, Norway. The NORESS array is a new densely spaced array, designed for coherent detection and analysis of high-frequency regional phases (Mykkeltveit et al, 1983) and consists of 25 vertical short-period sensors distributed in a circular area of 3 km aperture. The NORESS array, which has been operating since late 1984, is located near the 06C subarray of the older and larger NORSAR teleseismic array. NORSAR has 42 sensors in 7 subarrays distributed over a circular aperture of about 50 km. and has been recording data since 1971. The short-period NORSAR data is sampled at 20 Hz whereas the NORESS array, designed for the detection of high-frequency regional phases, samples data at 40 Hz.

Tables 1 and 2 give the source parameters of the earthquakes and explosions, recorded by NORESS located in western Norway. The earthquakes are those reported in the bulletins of the University of Bergen Regional Seismic Network. The locations are also plotted on a map in Figure 1. The tabulated local magnitudes were computed by the coda-duration method. The chemical explosions in Table 2 occurred at a known mine, A/S Titania, and Blasjo, which is a dam construction site, and had announced explosive yields in pounds. The origin times and local magnitudes are those reported in the Bergen bulletins. These earthquake and mine-blast locations are between 300 and 400 km north-northwest of the NORESS array.

The locations of mine blasts in northern Sweden and western Russia are given in Table 3 and are plotted on the map in Figure 1. The S2 Swedish event location was determined by the NORESS array, using the Regional Online Regional Event Processing Package (RONAPP), developed by Mykkeltveit and Bungum (1984). All the other source parameters were reported in the bulletin published by the Institute of Seismology at the University of Helsinki. The mine designations are those assigned to the different mines by Helsinki analysts as a result of the application of their manual location method. These events are located between 700 and 1000 km to the east of NORESS.

The locations of the presumed peaceful nuclear explosions (PNE's), given in Table 4 and plotted in Figure 2, were taken from the PDE bulletins. These events occurred before the NORESS array was operational but were large enough to be recorded by the NORSAR teleseismic array in the near-regional distance range (10 to 25 degrees).

Incoherent Beams. Short-period waveforms of regional seismic events can very complicated. We show the waveform characteristics of these events in the form of incoherent beams. Baumgardt (1985) has shown that incoherent or envelope beams are useful for analysing the overall shapes of complicated seismograms recorded at arrays. In brief, incoherent beamforming consists of computing the log-rms amplitudes in adjacent, one second time windows on each channel, starting about one minute before the P_n -wave onset time and extending through the seismogram into the L_g coda. Similar measurements are also made in two minutes of noise background to P_n . The one second log-rms estimates are then averaged over all the channels of NORESS and plotted versus time. The average noise levels are estimated over two minutes ahead of P_n and are plotted as horizontal lines. Incoherent beamforming smooths many of the amplitude fluctuations produced by local scattering and noise effects. This smoothing comes from the combined effects of time averaging over single-channel traces and stacking the traces

over all channels.

Figures 3 and 4 show incoherent beams for filtered waveforms of a western Norway earthquake and mine explosion, respectively, recorded at NORESS. The incoherent beams were formed after bandpass filtering each trace in 8 filter bands, 2.0-4.0, 2.5-4.5, 3.0-5.0, 4.0-6.0, 5.0-7.0, 6.0-8.0, 8.0-10.0, and 8.0-16.0 Hz., using third-order recursive Butterworth filters. Each trace and average-noise estimate has been artificially separated by 0.5 log-rms units for display purposes. Also, the major regional phases, P_n , P_g , S_n , and L_g are indicated along with the time windows used for spectral analysis, discussed below.

These beams show that significant energy is present in all phases to the 8-16 Hz frequency band. Another notable feature we have observed for western Norway earthquakes, such as the one in Figure 3, is the gradual emergence of P_n from the noise with increasing frequency. This is evident in Figure 3 where the P_n doesn't emerge from the noise until the 6-8 Hz filter. This appears to be a common feature of western Norway and North Sea earthquakes, as reported by Mykkeltveit (1985). The RONAPP processor at NORESS consistently underestimates distances to these events, relative to the Bergen locations, due to P_n being undetected and P_g used instead in making single-array locations. By comparison, however, the P_n wave stands out clearly in all filter bands for the incoherent beams of the Blasjo blast in Figure 4.

Figure 5 shows an example of a compressed incoherent beam plot for one of the PNE explosions recorded by NORSAR. In this case, the incoherent beam was computed by averaging five second log-rms amplitude estimates over all available NORSAR subarray channels. Because the PNEs are located at teleseismic distances ($\Delta > 10$ deg.) from NORSAR, most of the high-frequency energy beyond 5 Hz has been attenuated. Therefore, only a 0.6-3.0 Hz filter was applied. Also, in the case of the event in Figure 5, the first arrival is direct P rather than P_n . The P-coda window, used in lieu of the P_n and P_g windows, is indicated. Also, although this event is at 17.4 degrees from NORSAR, both S_n and L_g are clearly recorded.

Spectral and Cepstral Analysis. The cepstrum was first introduced in the early 1960's as a method of analyzing composite signals. It is defined as the Fourier transform of the logarithm of the spectrum (Bogart et al., 1963). This transform produces a function of delay time, or "queffrequency", which exhibits spikes at the time differences between the onset of the signal and any echos or repeated signals. Cepstral analysis has been used previously on seismic data for examining multiple events (Flinn, et al., 1973) and for depth estimation of events (Cohen, 1970; Kemerait and Sutton, 1982).

There are a number of variations of the cepstrum, including the complex, power and signed cepstra. The complex cepstrum is computed by taking the inverse Fourier transform of the complex logarithm of the spectrum (Oppenheim and Schaffer, 1975). It retains all phase information, so it should be used when a return to the time domain is necessary. The power cepstrum is the magnitude squared of the Fourier transform of the log power spectrum. It contains no phase information. The cosine-squared, or signed, cepstrum is the real part of the Fourier transform of the full symmetric log-power spectrum (Creede and Schneider, 1976). The signed cepstrum retains the phase information from the frequency domain, so it may contain positive and negative spikes. This permits better discrimination between spikes caused by multiple-source events and those caused by reflection echos. Reflections, such as p^l or s^l , produce negative fundamental spikes due to Lloyds mirror effect (Creede and Schneider, 1976). The signed cepstrum was used in this study because no return to the time domain was required and detection of delayed signals which have the same polarity was desired.

In computing the power spectra of the different phases, an array stacking procedure was used to obtain smooth spectra. The stacking process cancels out uncorrelated noise and scattering effects in single channels and is essentially the frequency-domain equivalent to time-domain incoherent beamforming. In this study, array stack spectra were obtained using a procedure similar to that described by Bache et al (1985) and Tang and Alexander (1985). The Fourier power spectrum of each windowed phase and the pre- P_n noise is first computed on each array channel. The window lengths varied depending on the duration of each phase, but in general were between 7 and 14 seconds for P_n , P_g , and S_n , and 25.6 seconds for L_g and noise for the regional events recorded at NORESS. In the case of the NORSAR recordings of the PNEs, 51.2 second windows were used on the P-coda, S_n , and L_g phases and on the noise ahead of P. These phase windows are shown at the top of Figures 3, 4, and 5. The spectra for each phase and noise on each channel were smoothed with cosine and Hanning windows, and the resulting channel spectra were then averaged across the arrays. The average spectra were then corrected for the instrument by spectral division and for noise by subtracting the noise power spectrum frequency by frequency from the power spectrum of each phase.

Also, for the NORSAR seismograms of PNEs, a source correction was made to the spectra. The explosion source model of von Seggern and Blandford (1972) was used assuming an explosion medium of granite. The yield was estimated assuming the m_b values in Table 4 to be proportional to 0.9 times the yield.

Some additional processing of the log power spectrum was required before computing the cepstrum. First, after correcting the power spectrum for instrument and noise, the logarithm was computed. If the signal spectral density fell below that of the noise at high frequency, the last good value of the spectrum was extended out to the Nyquist frequency. We found that this reduced the ringing in the cepstrum which occurred because of the high-frequency oscillations in the noise. Second, the spectrum becomes very large at very low frequency because of the removal of the instrument response. To correct this, the spectral values below a cutoff frequency, 1 Hz for NORSAR and 2 Hz for NORESS, were set to the cutoff-frequency spectral value. Third, the mean and linear trend in the log power spectrum were then removed. Finally, the log spectrum was reflected about the Nyquist frequency to produce the full symmetric log-power spectrum. This symmetric spectrum ensures that all of the information is in the real part of the Fourier-transform output.

SPECTRAL/CEPSTRAL ANALYSIS RESULTS

Western Norway Events. Figure 6 shows the spectra for the six earthquakes shown on the map in Figure 1. Each plot consists of the spectra for the regional phases, P_n , P_g , S_n , and L_g , for the windows shown in Figure 2. The P_g , S_n , and L_g spectra have been shifted up, respectively, by 0.5, 1.0, and 1.5 units relative to the P_n spectra for display purposes. The dashed line on the bottom of each is the pre- P_n noise spectrum. Note that the P_n spectrum has not been shifted relative to the noise spectrum. Also, it should be recalled the signal spectra have been corrected for noise by spectral subtraction. Thus, comparison of the noise-corrected signal spectra and the noise spectra indicates the true signal-to-noise ratio for P_n . Moreover, whenever noise correction results in a negative spectral density, the noise-corrected signal density is set to the noise value. Thus, if the P_n spectra falls on the noise spectrum for several frequencies, the signal does not exceed the noise level at those frequencies. However, it is possible for the noise-corrected signal amplitudes to be less than the noise amplitudes. For example, the P_n spectral nulls which fall below the noise spectrum in Figure 6 represent signal-to-noise ratios which are less than one.

One common feature of all the earthquake P_n spectra in Figure 6 is that there is no P_n signal energy at frequencies less than 4 Hz. The P_n spectra appear to be peaked between 8.0 and 20.0 Hz with a strong spectral null somewhere below 4.0 Hz. This observation agrees with the filtered incoherent beam analysis, discussed above and shown at the top of Figure 3, where P_n energy only appears on incoherent-beam traces with filters above 8 Hz. The P_g , S_n , and L_g spectra all exhibit energy above the noise levels at around 2.0 Hz which decreases linearly with frequency. It is also interesting to note that, with the exception of event Q6, which seems to have a spectral null at between 2 to 3 Hz, the P_g and L_g spectra are almost parallel with nearly the same spectral decay slope, whereas the S_n spectra appear to decay at a slower rate. In fact, at frequencies above 8 Hz, the P_n and S_n spectra are very similar in slope. This suggests that common attenuation mechanisms are responsible for the P_n , S_n and P_g , L_g spectral decays, and that the attenuation of P_n and S_n is less than that of P_g and L_g .

Figure 7 shows the spectra for the six western Norway blasts, 3 (NM1, NM2, NM3) at the Blasjo site and 3 (NM4, NM5, and NM6) at the Titania mine. Comparing these spectra with the earthquake spectra in Figure 6 reveals that the explosion spectra are more complicated. The complications are caused by modulations or scalloping in the spectra. The nulls of the modulations occur at nearly the same frequencies for the spectra of different phases, which is a clear indication that the scalloping results from source multiplicity. Of course, modulations of this kind can be produced by multipath phases or depth phases interfering with the primary phases. Such interference may be expected for P_n , but not for L_g , and the interference patterns in the spectra would not be identical, as they are in Figure 7. Also, the P_n spectra have increased signal-to-noise ratio at frequencies below 8 Hz compared with the earthquakes in Figure 6. This result is also consistent with the incoherent beam analysis in Figure 4, where strong P_n energy is apparent in all frequency bands.

Figure 8 shows the cepstrums for the earthquakes, computed by Fourier transforming the spectra in Figure 6 using the methods discussed in the previous section. Only quefrequencies out to 0.6 seconds are displayed. The cepstrum for each phase has been shifted in units of 0.05 for display purposes. The P_n cepstrum is unshifted. Also, the parallel dashed lines, labeled for each phase, indicate the zero levels for the shifted cepstrums corresponding to that phase. Thus, any cepstral value which falls below the dashed line indicates a negative cepstral

amplitude. Some peaks can be observed in these cepstra, the strongest ones appearing in the low-quefrequencies of the Pn phase. However, most of the cepstra are simple, particularly the Lg cepstra, which have nearly zero cepstral values at all quefrequencies.

The cepstrums for the 6 explosion spectra in Figure 7 are plotted in Figure 9. In contrast to the earthquake cepstra, the mine-blast cepstra exhibit a number of very significant peaks, indicated by the superimposed arrows. For a given event, the quefrequencies of the major peaks are nearly the same, which is a manifestation of the identical spectral-modulation patterns, pointed out above, in the spectra in Figure 7.

In the theoretical discussion above, we showed that delayed explosions would result in modulated spectra, with the spacing of the peaks and troughs in the modulations determined by the one over the delay time, τ . For a single delay, the power spectrum would have one single modulation of $\frac{1}{\tau}$ (Equation 2). However, the log of the power spectrum would have higher-order modulations. The strongest secondary modulation would have periodicity of $\frac{1}{2}\tau$ and its amplitude would be negative (Equation 5). Thus, the cepstrum for a single delay should have a positive peak at a quefrequency of τ followed by a negative peak at a quefrequency of 2τ . There would then follow other secondary peaks at integer multiples of τ , but their amplitudes would decay rapidly with quefrequency.

Examination of Figure 9 shows that explosions NM2, NM5, and NM6 may have been single-delay shots. NM5 has main peaks at about 0.04 seconds and a secondary negative peak at 0.08 seconds, or 2 times, which would indicate a single delay of 40 milliseconds. However, we believe that they may be processing artifacts, caused by the detrending and reflection of the spectrum at 20 Hz. The spacing between nulls in the NM5 spectra in Figure 7 is on the order of 8 or 9 Hz corresponding to the peak in the NM5 cepstrum in Figure 9 at about 0.11 seconds, indicated by the first arrow. There is also a very weak trough, pointed out by the second arrow, at about 2 times 0.11 seconds, or 0.22 seconds. Thus, we would interpret event NM5 as being two blasts delayed by about 111 milliseconds.

For NM6, there is a primary positive peak at about 0.15 and a smaller negative peak at 0.3 seconds, consistent with a single delay of 150 milliseconds. This seems to be consistent with the NM6 spectrum in Figure 8, which has at least two modulations with nulls separated by about $\frac{1}{0.15}$ or 6.7 Hz. The NM2 cepstra are the simplest of those in Figure 9, with a primary peak at about 0.08 seconds and the secondary negative trough at about 0.14 seconds, which suggests a single delay of 80 milliseconds. This corresponds to the a broad modulation in the NM2 spectrum in Figure 8 of about $\frac{1}{0.08}$ or 12.5 Hz.

The cepstra for events NM1, NM3, and NM4 are more complicated with more than one peak and trough, indicated by the solid arrows. From equations 8 and 9 and simulation studies, discussed below, these multiple peaks appear to be an indication that these explosions consist of two or more combinations of blasts. The quefrequencies of the primary peaks vary from event to event, but in general, they tend to be between 0.08 and 0.15 seconds. These are consistent with multiple explosions with delays on the order of 80 to 150 milliseconds. All these delays, including the single delay blasts, appear to be the fast or millisecond-type, mine-blast delays, discussed above.

Swedish and Russian Mine Blasts. Figure 10 shows spectra for the three mine blasts in northern Sweden and the two mine blasts near Leningrad, whose locations are tabulated in Table 3 and plotted in Figure 1. As with the western Norway spectra, the Pg , Su , and Lg

spectra have been shifted up respectively by 0.5, 1.0, and 1.5 units relative to the P_n and noise spectra for display purposes. Although these events are about twice the distance from NORESS as the western Norway events, they still have significant energy in all phases out to frequencies of 16 to 18 Hz.

The spectra of the Swedish events, SM2, SM3, and SM1, are very complicated with modulations although these modulations are the same for all the phases. Since these modulations do not appear in the noise spectrum, they must be due to the signal characteristics and not to the low signal-to-noise ratios. Particularly striking in the SM1 and SM3 spectra is the large broad spectral peak at about 9 or 10 Hz. SM2 also has broad peak at about 8 Hz.

The spectra of the Russian blasts, LM2 and LM1, are simpler than the Swedish events although spectral modulations can be easily seen and are nearly identical in all phases. However, the spectral periodicity of the modulations is greater than that of the Swedish spectra and more closely resemble the western Norway mine-blast spectra in Figure 7. In fact, the spectra for the BLA mine blast NM2, in Figure 7, are very similar to those of LM2. They both exhibit two broad cycles with nulls separated by about 12 Hz.

The cepstra for the spectra in Figure 10 are shown in Figure 11. As might be expected, the cepstra of the Swedish mine blasts SM2, SM3, and SM1 are very complicated with many peaks and troughs, indicated by the arrows. SM3 and SM1 have strong peaks at about 0.1 seconds quefrequency, which probably corresponds to the 9 to 10 Hz spectral modulation pointed out above. These events seem to consist of more than two blasts, although the basic delay time is probably on the order of 100 milliseconds.

The cepstra for event LM2 has a positive peak between 0.06 and 0.08 seconds, which appears to correspond to the broad loop with nulls separated by about 12 Hz in the spectra in Figure 10. There is also a trough near 0.12 seconds, which is almost twice the quefrequency of the main peak. Therefore, we interpret LM2 as being two explosions separated in time by about 80 milliseconds, like the NM2 BLA mine blast discussed above.

The LM1 cepstra contain more peaks at higher quefrequencies than the LM2 cepstra. The LM1 spectra in Figure 10 consist of about two loops, the first having nulls spaced apart by about 6 Hz and the second by about 7 or 8 Hz. These loops should produce positive cepstral peaks between 0.125 and 0.17 seconds quefrequency and negative peaks at between 0.25 and 0.34 seconds. As shown by the arrows in Figure 11, broad peaks are visible at these quefrequencies in the LM1 cepstra. However, strong peaks are also visible at quefrequencies below 0.1 seconds. The origin of these peaks is not clear from the spectra in Figure 10, since there do not appear to be broad modulations with nulls separated by 10 Hz. or greater. Processing artifact, possibly as a result of removing the linear trend, may have caused a humped spectrum of 20 Hz breadth which could have caused the peaks near 0.05 seconds. We therefore conclude that LM1 consists of at least two explosions, separated by between 125 and 170 milliseconds.

Western Russia PNEs. The NORSAR spectra for the presumed PNEs in western Russia are shown in Figure 12. These spectra were computed in the same manner as the NORESS spectra, however, none of the spectral plots in Figure 12 have been shifted for display purposes. Because these events are at distances beyond 10 degrees, these spectra do not contain the same high-frequency content as the regional signals recorded at NORESS. The NORSAR short-period antialias filter cuts off frequencies above 5 Hz, so we have only plotted the spectra to 5 Hz. Clearly, the reduced bandwidth for these teleseismic signals makes it impossible to resolve millisecond delays in mine blasts. Only delays of 200 to 300 milliseconds or greater will be resolvable with the 5 Hz bandwidth of the short-period NORSAR data.

Examination of the spectra in Figure 12 reveals modulations like those observed in the mine blasts at NORESS, except the PNE modulations have much shorter spectral periodicity. All the spectra have a low-frequency spectral null between 1 and 2 Hz. The frequency of the first spectral null is different for different events, but the same in the spectrum of each phase (P coda, S_n , and L_g) for each event. Spectral modulations are clearest in the P-coda spectra which have the most high-frequency content. The S_n and L_g spectra roll off faster with frequency and have less high-frequency content than the P-coda spectra. Because of this, spectral nulls are less obvious above 2 Hz in the S_n and L_g spectra than in the P-coda spectra. Also, as in the case of the NORESS recordings of mining explosions, the nulls do not appear in the noise spectra, and thus the signal spectral nulls cannot be due to noise contamination.

Events E2 and E6 show the clearest evidence of spectral nulls throughout the entire frequency band in the spectra of all three phases. For E2, the nulls appear at between 1.75 to 2.0 Hz, about 3.5 Hz and near 5.0 Hz. The nulls in the E6 spectra occur at between 1.0 and 1.5 Hz, about 3.0 Hz, 4.0 Hz, and near 5.0 Hz. For the other events, after the first null, the S_n and L_g spectra have one hump or peak which is about the same as those in the P-coda spectra. After the first cycle, the modulation pattern in the S_n and L_g spectra seems to be obscured as the signal-to-noise ratio decreases with increasing frequency. However, in all cases, there is an approximate correspondence in the location of the nulls of the spectral modulations, at least for the first cycle, for all phases. Thus, the signals from these events appear to have been produced by more than one explosion.

The cepstra for these events, plotted in Figure 13, have peaks and troughs at similar frequencies for all three phases. However, they are not as sharp and well defined as those in for the mine blasts recorded at NORESS because of the reduced bandwidth at NORSAR and the fact that the nulls in Figure 12 are not as deep as those for the mine blasts recorded at NORESS. The cepstral peaks below 0.4 seconds frequency are due to processing artifact. In particular, the peak near 0.2 seconds in most of the cepstra is due to the reflection of the spectra at 5 Hz prior to computing the cepstra.

Event E3 has the sharpest cepstral peaks because the spectral nulls in the E3 spectra in Figure 12 are the deepest of all the spectra, particularly in the P-coda spectrum. The strongest P-coda peak for E3 is at about 1 second frequency. A strong peak also appears at about 1 second in the L_g cepstrum and a smaller peak in the S_n cepstrum at a frequency slightly less than 1 second. The slight shift in the peak frequencies seems to be due to noise contamination in the S_n and L_g spectra, and we interpret E3 as being composed of two explosions delayed by about 1 second.

The E2 cepstrum has the most consistent set of peaks in all phases at about 0.75 seconds frequency, as indicated by the arrow. Event E1 has a set of somewhat less clear peaks at a frequency of about 0.9 seconds. Events E4 and E6 have peaks between 0.6 and 0.8 seconds, although are negative. These troughs may be due to noise contamination and processing artifact.

Event E5 has a particularly strong peak in the P-coda cepstrum at about 1.4 seconds, caused by the very strong spectral modulation, evident in the E5 P-coda spectrum in Figure 12, with peak and trough separations of about 0.7 Hz. The first cycle of this modulation can be seen in the S_n and L_g spectrum, but then disappears at higher frequency due to noise contamination. This one cycle does not appear to be sufficient to produce strong cepstral peaks in the S_n and L_g cepstra in Figure 13. However, based on the strength of the modulation in the P-coda spectrum and the fact that part of the modulation appears in the low-frequency part of the S_n and L_g spectra in Figure 12, we conclude that event E6 is two explosions delayed by 1.4

seconds.

SIMULATION EXPERIMENTS

In order to obtain a better understanding of the spectral characteristics of multiple explosions, we simulated multiple explosions using signals of one of the western Norway earthquakes. Event Q1 was used since its spectrum did not have modulations and thus appears to be single event, at least within the resolution of the NORESS bandwidth. Thus, if the signals from Q1 were produced by a set of events with constant delay time, the delay times would have to be less than $\frac{1}{20}$ Hz, or 50 milliseconds.

Assuming that the Q1 signals are from a single explosion, we built up a simulated multiple explosion by using the Q1 signals delayed in time and with different amplitude, numerically simulating equation 6. The signal was first isolated from the first onset of the P_n to well into the L_g coda. The noise ahead of the P_n onset was retained and assumed to be the noise ahead of the multiple explosion. Thus, the isolated signal was added to the original seismogram, but delayed in time and multiplied by some amplitude factor, α . This can be done more than once to produce a composite multiple-event sequence. We then computed spectra and cepstra of the resultant simulated multiple-event signal as we did with the NORESS data.

The spectra of four simulations are shown in Figure 14. The corresponding cepstra for these spectra are plotted in Figure 15. Figure 14(a) is the spectrum for two events, separated by 125 milliseconds, and having the same amplitude. The resultant spectra have very deep nulls, separated by $\frac{1}{125}$ milliseconds, or 8 Hz. These spectra resemble the deep-null spectrum of the Russian mine blast, LM1 (Figure 10), and the PNE E3 (Figure 12), although the spacing of the nulls of E3 are much less than those of the simulation. However, most of the spectra do not exhibit the deep nulls characteristic of this simulation. The corresponding cepstrum in Figure 15(a) shows a clear peak at 0.125 seconds quefrency, as expected. Also, note the smaller negative peak at twice the delay time, or 0.25 seconds.

Figure 14(b) shows the effect of superimposing three delayed events, according to the following

$$y(t) = \alpha_1 x(t) + \alpha_2 x(t-\tau) + \alpha_3 x(t-2\tau), \quad (10)$$

where $\alpha_1 = \alpha_2 = \alpha_3 = 1$ and $\tau = 0.125$ seconds. The number of cycles in the spectra have been doubled, relative to the single delay case, and the widths of the cycles have been halved. There are still two dominant peaks, one at 8 Hz and one at 16 Hz, separated by 8 Hz, which is the reciprocal of the delay time, 0.125 seconds. The cepstra of this case, in Figure 15(b), still have strong positive peaks at 0.125 seconds and an additional peak at twice 0.125 seconds, or 0.25 seconds.

Figure 14(c) shows the resulting spectra for the case when $\alpha_2 = \alpha_3 = 0.5\alpha_1$ in equation 10, that is, for three delayed explosions with the second and third explosions being half the amplitude of the first. The delay time is still 0.125 seconds. Changing the relative amplitudes of the different delayed signals makes the nulls less deep and the spectral modulations less obvious. The cepstral peaks in Figure 15 for this case are weaker than for the case when the signals were the same amplitude. The cepstra are in general simpler when the delayed-signal amplitudes are different, and the higher quefrency interference peaks are much less apparent. This simulation resembles most of the cases we have studied, especially NM5, NM6, and NM2 in Figure 7, LM2 in Figure 10, and all the PNE examples, except E3, in Figure 12. Thus, it

appears that most delayed explosions are composed of explosions of different sizes.

Finally, Figure 14(d) shows the case of 30 superimposed signals each delayed by 0.125 seconds. Comparing this case with the 3 signal simulation in Figure 14(b), we see that main peaks at 8 and 16 Hz begin to dominate relative to the secondary lobes. Clearly, in the limit as the number of explosions approaches infinity, the main peaks become delta functions. Figure 15(d) shows that the cepstra for this case consists of of the primary peak at 0.125 seconds and many secondary peaks. None of the spectra or cepstra we have examined so far resemble this case. Thus, it appears that all of delayed explosions we have studied consist of, at most, 3 or 4 explosions.

It should be noted that these results do not preclude the possibility of there being shorter delays than 50 milliseconds. In fact, in the case of the mining explosions, each explosion delayed by milliseconds is probably a salvo of several charges delayed by intervals of 25 to 50 milliseconds or less (Dick, et al, 1983). Delays this short could not be resolved by any of the data used in this study. Bandwidths on the order of 80 Hz or greater would be required to resolve delays shorter than 25 milliseconds.

DISCUSSION AND CONCLUSIONS

This study has shown that the effects of ripple firing in mine blasts and PNEs can be resolved from the analysis of the high-frequency spectra of different phases. The best explanation for a consistent modulation pattern persisting in the spectra of all phases in a seismogram is that the signals are a composite of two or more delayed signals. Although it is true that multipathing effects, such as P - pP interference, can also cause modulations, they would produce different modulations for different phases. Moreover, it is unlikely that such effects would be observed in Lg and Lg -coda spectra.

We have used cepstral analysis to make an estimate of the delay times between explosions. This has sometimes proved difficult because of the limited bandwidth available in the NORESS spectra, and in particular, in the NORSTAR spectra. However, our estimates of delay times have been consistent with the fast or millisecond type delays commonly used in underground mines. These delay times are consistent with the known blasting practice in the Norwegian mines, where delays on the order of 100 to 150 milliseconds are common (S. Mykeltveit, personal communication).

For the PNEs, our results indicate much longer delays, on the order of 0.75 to 1.25 second delays. Because these explosions are much larger than the mine blasts, as evidenced by their higher body-wave magnitudes, they are probably being used to move much larger volumes of rock. The Soviet Union has given only a limited amount of information about their PNE program. What information is available in the Soviet literature indicates that the PNE program is primarily directed toward various economic development applications (Nordyke, 1983). For example, many of the explosions in the Pechora River region and around the Ural Mountains, which are the regions where the PNEs used in this study occurred, appear to have been fired near major river systems in order to redirect their flow southward through canal systems to the more arid parts of the Soviet Union (Nordyke, 1974). However, recent reports in the scientific press indicate that the Soviet Union has discontinued these projects because of their likely deleterious impact on the environment (Dickson, 1986). These shots may have been delayed in order to enhance the fracture efficiency of the explosions and also to reduce ground motion effects. As we discussed earlier, explosion delay times should increase for larger explosions. Thus, given the size of these explosions and the magnitude of the project the Soviets may have been attempting, the 0.8 to 1.25 second delay times appear to be reasonable.

From visual analysis of spectra and cepstra, we have not been able to unequivocally ascertain the number and sequence of delayed explosions. The temporal pattern of multiple-explosion signals is determined not only by the time sequencing of the explosions but also how they are arranged spatially. From our theoretical and simulation analyses, we have found that more than two interfering signals can produce very complex log spectra and signed cepstra. In order to determine the exact pattern of explosions in our data, it would be necessary to make simulations, generate theoretical spectra and cepstra, and find those which most closely resemble the observed data. In order to infer anything about the spatial pattern of explosions, spectral observations from several different azimuths around the mine would be required. Such an inversion scheme would be the spectral equivalent to time domain studies of complex earthquakes, such as that of Barker and Langston (1981).

These results also have significance for discrimination between mine blasts and earthquakes. Although we have clearly observed differences between mine blasts and earthquakes in western Norway, these differences are mainly a consequence of mine blasting practice. We also

observed a spectral difference in the P_n spectra, where earthquake P_n spectra seem to be peaked between 8 and 16 Hz with little energy below 4 Hz whereas the explosions have flatter spectra. One possible explanation of this difference in P_n excitation is that the western Norway earthquakes may occur at greater depth in the crust than the near-surface mine blasts, and thus, pP_n may partially cancel P_n energy at frequencies below 4 or 5 Hz. However, we do not now know for sure if this difference is due to intrinsic source differences or to path differences. As long as mine-blast ripple firing is used, mine blasts can be distinguished from earthquakes by looking for modulations and nulls in the explosion spectra. Mine blasts almost always consist of delayed explosions, although the delay times will vary depending on what is being accomplished. However, we have not always observed millisecond delays in blasts in the Leningrad region. There are undoubtedly shorter delay explosions used, with delays less than 50 milliseconds, which cannot be resolved with the 40 Hz sampled NORESS data.

Another important consideration is whether chemical mine blasts can be distinguished from nuclear explosions. If mine blasting always uses ripple firing (This could be required in the negotiated protocol of a comprehensive test ban treaty.), high-frequency data are available, and nuclear tests do not have delays, then it can be done. In order to make a nuclear-weapons test look like a mine blast, it would be incumbent on the testban treaty violator to simulate the ripple fire of mine blasting. We have shown in this study that PNEs in western Russia appear to be multiple shots, although the delays are greater than the mine blasts. However, it may be expensive and difficult to always simulate very short delays. Another possibility would be to set off a string of chemical explosives and time a nuclear explosion to be in the string sequence. Such a blast may stand out strongly as compared with mine blasts which may be discernable in the spectra.

Future research should address the use of higher frequency data for the resolution of much shorter delays. Recently, the High Frequency Seismic Element (HFSE) has been installed at NORESS (Ringdal, et al, 1986) which provides the high frequency data needed for such a study. The HFSE element consists of a Geotech S-3 seismometer in a 60 m borehole, at the NORESS center, and is sampled at 125 Hz. Ringdal et al (1986) have found that this element provides data which have good signal-to-noise ratio in P_n and P_g spectra out to 62.5 Hz. for events at distances out to 500 km from NORESS. Thus, with these data, it should be possible to resolve explosion delays of 25 milliseconds and less for the mines in western Norway.

ACKNOWLEDGEMENTS

The NORSAR and NORESS data used in this study were provided by Frode Ringdal and the NORSAR staff. We wish to thank Frode Ringdal and Sven Mykkeltveit for many useful discussions about Scandinavian seismology and NORSAR and NORESS data processing. We also owe thanks also to Richard Dick of the Bureau of Mines for a very enlightening discussion about mine blasting practice and to Robert Kemerait for helpful advice in doing cepstral analysis. This research was partially supported under DARPA contracts F19628-85-C-0057, monitored by Air Force Geophysics Laboratory, and MDA903-86-C-00073, monitored by Defense Supply Service.

REFERENCES

- Aviles, C.A. and W.H.K. Lee (1986). Variations in signal characteristics of small quarry blasts and shallow earthquakes, Abstract in *EOS, Transactions of the American Geophysical Union*, **67**, 1903.
- Bache, T.C., P.D. Marshall, and L.B. Bache (1985). Q for teleseismic P waves from central Asia, *J. Geophys. Res.*, **90**, 3575-3587.
- Barker, J.S. and C. Langston (1981). Inversion of teleseismic body waves for the moment tensor of the 1978 Thessaloniki, Greece, earthquake, *Bull. Seism. Soc. Am.*, **71**, 1423-1444.
- Baumgardt, D.R. (1985). Comparative analysis of teleseismic P and Lg waves from underground nuclear explosions in Eurasia, *Bull. Seism. Soc. Am.*, **71**, 1413-1433.
- Bell, A.G. and S.S. Alexander (1977). Abstract in *EOS, Transactions of the American Geophysical Union*, 58.
- Bogart, B.P., M.J.R. Healy and J. Tukey (1963). The frequency analysis of time series echoes: cepstrum, pseudo-autocovariance, cross-cepstrum, and phase-cracking, *Proceedings on the Symp. on Time Series Analysis*, M. Rosenblatt ed., Wiley, New York. 209-243.
- Cohen, T.J. (1970). Source-depth determinations using spectra, pseudo-autocorrelation, and cepstral analysis, *Geophysics J.*, **20**, 223 - 231.
- Creede, G.D., and S.M. Schneider (1976). Signed Cepstragram Program for the OTS/RATHION 704 Computer, *Report No. 0438-76-4*, ENSCO, Inc., Springfield, Virginia.
- Dick, R.A., L.R. Fletcher, and D.V. D'Andrea (1983). *Explosives and Blasting Procedures Manual*, Information Circulation 8925, Bureau of Mines, United States Department of the Interior.
- Dickson, D. (1986). Soviet Union suspends plans to divert four rivers, *Science*, **233**, 1036.
- Flinn, E.A., T.J. Cohen, and D.W. McCowan (1973). Detection and analysis of multiple seismic events, *Bull. Seism. Soc. Am.*, **63**, 1921 - 1936.
- Gupta, I.N., J.A. Burnett, R.A. Wagner, and M. Marshall (1984). Discrimination between quarry blasts, nuclear explosions, and earthquakes, *TGAL-TR-84-1*, Teledyne Geotech, Alexandria, Virginia.
- Kemerait, R.C., and A.F. Sutton (1982). A multidimensional approach to seismic depth estimation, *Geoexploration*, **20**, 113 - 130.
- Langefors, U. and B. Kihlstrom (1963). *The modern technique of rock blasting*, Almqvist and Wiksells Boktryckeri Aktiebolag, Uppsala, Sweden.
- Murphy, J.R., and T.J. Bennett (1982). A discrimination analysis of short period regional seismic data recorded at Tonto Forest Observatory, *Bull. Seism. Soc. Am.*, **72**, 1351-1366.
- Mykkeltveit, S. (1985). Evaluation of NORESS real-time processing performance: case study for 132 western Norway/ North Sea events, *Semiannual Technical Summary*, 1 April -

30 September 1985. NORSAR, Kjeller, Norway.

- Mykkeltveit, S., K. Astebol, D.J. Doornbos, and E.S. Husebye (1983). Seismic array configuration optimization, *Bull. Seism. Soc. Am.*, **73**, 173-186.
- Mykkeltveit, S. and H. Bungum (1984). Processing of regional seismic events using data from small-aperture arrays, *Bull. Seism. Soc. Am.*, **74**, 2313-2333.
- Nordyke, M.D. (1974). A Review of Soviet Data on the Peaceful Uses of Nuclear Explosions, *URCL-51414*, Lawrence Livermore Laboratory, Livermore, California.
- Nordyke, M.D. (1983). The test ban treaties: Verifying compliance, *Energy and Technology Review*, Lawrence Livermore Laboratory, Livermore, California.
- Oppenheim, A.V., and R.W. Schaffer (1975). *Digital Signal Processing*, Prentice-Hall, Inc., New Jersey.
- Papageorgiou, A.S. and K. Aki (1983a). A specific barrier model for the quantitative description of inhomogeneous faulting and the prediction of strong ground motion, *Bull. Seism. Soc. Am.*, **74**, 953-978.
- Papageorgiou, A.S. and K. Aki (1983b). A specific barrier model for the quantitative description of inhomogeneous faulting and the prediction of strong ground motion. Part II. Applications of the model, *Bull. Seism. Soc. Am.*, **73**, 953-978.
- Ringdal, F., B.Kr. Hokland, T. Kvaerna (1986). Initial results from the NORESS high frequency seismic element (HFSE), *Semiannual Technical Summary*, 1 October - 31 March 1986, NORSAR, Kjeller, Norway.
- Tang, L. and S.S. Alexander (1985). Estimates of average Q for L_g propagation in Eurasia, *EOS, Trans. Am. Geophys. Union*, **66**, 305.
- von Seggern, D.H. and R.R. Blandford (1972). Source time functions and spectra for underground nuclear explosions, *Geophys. J. R. astr. Soc.*, **31**, 83-97.

FIGURE CAPTIONS

Figure 1. Map showing locations of the western Norway earthquakes, the Blasjo (BLA) and Titania (TITA) mines, mines in northern Sweden, and Leningrad-region mines and the NORESS regional array. Locations of the western Norway earthquakes are from the bulletin of the Western Norway Seismic Network of the University of Bergen. BLA and TITA locations are the known mine locations. The Swedish and Leningrad mine locations come from the bulletin of seismicity in the Nordic countries published by the Seismological Institute of the University of Helsinki.

Figure 2. Map showing PDE locations of the presumed PNEs in western Russia and the NOR-SAR teleseismic array.

Figure 3. Filtered incoherent beams of one of the BLA mine blasts (NM1 in Table 1) in western Norway. Incoherent or envelope beams are computed by averaging across the NORESS array the average log-rms amplitudes computed in 1 second windows on each channel. Horizontal lines are the log-rms noise levels averaged over 2 minutes before P_n onset time. Filters are third-order Butterworth recursive filters designed to realize the bandpass frequencies indicated. Each plot for different filters has been shifted by 1.0 log-rms unit for display purposes. P_n , P_g , S_n , and L_g windows used in spectral analysis are shown at the top.

Figure 4. Same as Figure 3 for one of the western Norway earthquakes (Q6 in Table 2). Diminished P_n amplitude at low frequency and its emergence at frequencies above 4 Hz are apparent.

Figure 5. Incoherent beam plot for a western Russia PNE (E2 in Table 4). Log-rms amplitudes are computed in 5 second windows on each channel and averaged across the NORSAR array. The P-coda, S_n , and L_g windows used in spectral analysis are indicated.

Figure 6. NORESS array-average spectra for each phase, P_n , P_g , S_n , and L_g , from the western Norway earthquakes. The pre- P_n noise spectrum is plotted with a dotted line. Each spectrum has been corrected for instrument and pre- P_n noise. The spectra of P_g , S_n , and L_g were respectively shifted by 0.5, 1.0, and 1.5 units relative to the P_n spectra. The P_n spectrum is not shifted relative to the noise spectrum.

Figure 7. NORESS array-average spectra for the western Norway mine blasts. The spectra were computed the same as those in Figure 6.

Figure 8. Signed cepstra for the western Norway earthquakes, computed by the forward Fourier transform of the spectra in Figure 6. Each spectrum in Figure 6 was detrended, zero-meaned, and reflected about the 20 Hz point before Fourier transforming. The P_g , S_n and L_g cepstra have been shifted respectively .05, .1, and .15 units relative to the P_n cepstrum. The dashed, horizontal lines are the zero levels for each of the phases, which are labelled to the right.

Figure 9. Signed cepstra for the western Norway mine blasts, computed by the forward Fourier transform of the spectra in Figure 7 with the same preprocessing as the cepstra in Figure 8. Arrows indicate the locations of peaks which appear at the same quefrequencies in all phases and discussed in detail in the text.

Figure 10. Spectra for the northern Sweden mine blasts (SM1, SM2, and SM3) and mine blasts near Leningrad (LM1 and LM2).

Figure 11. Signed cepstra for the northern Sweden mine blasts and mine blasts near Leningrad, computed by Fourier transforming the spectra in Figure 10. Arrows indicate the quefrequencies of the significant cepstral peaks, related to the modulations in the spectra in Figure 10, discussed in the text.

Figure 12. NORSAR array-averaged spectra for the PNEs listed in Table 4. Spectra are for P-coda, S_n , and L_g in 51.2 second windows, shown in Figure 5, and the noise spectrum, for a 51.2 second window before the P onset, is plotted with a dotted line. These spectra were computed in the same manner as the NORESS spectra, except an additional source correction was also applied, discussed in the text. The spectra are not shifted relative to each other or the noise spectra.

Figure 13. Signed cepstra for the PNEs computed by Fourier transforming the spectra in Figure 12. The S_n and L_g cepstra have been shifted up by 0.05 and 0.1 units, respectively, relative to the P-coda spectra for display purposes. The dotted lines indicate the shifted zero levels for the cepstrum of each phase. Arrows indicate frequencies of significant peaks related to the modulations in the spectra in Figure 12, which are discussed in the text.

Figure 14. Spectra for the multiple-source simulation using the signals from the Q1 earthquake. (a) Spectra for composite of the 2 Q1 seismograms added together but the second seismogram delayed by 125 milliseconds relative to the first. (b) Spectra for 3 Q1 seismograms added together but delayed by 125 milliseconds. (c) Same as (b), but with the second and third seismograms reduced in amplitude by 0.5 relative to the first. (d) Spectra for composite of 30 Q1 seismograms added together with delays of 125 milliseconds and with the same amplitudes.

Figure 15. Signed cepstra for the simulated multiple explosions computed by Fourier transforming the spectra in Figure 14. The cepstra in (a), (b), (c), and (d) correspond to the spectra in Figures 14(a), 14(b), 14(c), and 14(d), respectively.

EVENT	DATE (m/d/y)	ORIGIN TIME (UTC)	LATITUDE (deg N)	LONGITUDE (deg E)	M_L
Q1	2/05/86	20:23:15.9	62.66	4.61	2.7
Q2	2/05/86	23:35:41.1	62.74	4.50	2.6
Q3	2/06/86	06:19:52.4	62.90	4.86	2.3
Q4	2/13/86	19:03:48.2	62.61	5.07	2.6
Q5	2/13/86	13:39:00.3	62.40	5.28	2.5
Q6	2/16/86	18:19:41.3	61.69	4.90	2.0

EVENT	DATE (m/d/y)	ORIGIN TIME (UTC)	SIZE (TONS)	M_L
<i>BLASJO MINE EXPLOSIONS</i> (LAT. = 59.31 deg N LONG. = 6.950 deg E)				
NM1	08/05/85	17:42:58.7	62.9	2.6
NM2	08/06/85	17:50:07.9	30.8	2.4
NM3	10/17/85	10:00:00.4	32.7	2.4
<i>TITANIA MINE EXPLOSIONS</i> (LAT. = 58.342 deg N LONG. = 6.425 deg E)				
NM4	11/08/85	14:18:54.6	132.5	2.4
NM5	02/14/86	14:13:24.9	95.7	2.7
NM6	02/14/86	17:54:10.6	16.2	2.3

TABLE 3							
EPICENTERS FOR EVENTS EAST OF NORESS							
EVENT	MINE	DATE (m/d/y)	ORIGIN TIME (HR:MN:SEC)	LAT (deg N)	LONG (deg E)	M_L	SOURCE
<i>NORTHERN SWEDEN MINES</i>							
SM1	R1	12/16/85	14:44:36	67.1	20.6	2.5	Helsinki
SM2	-	01/28/86	10:18:33	66.0	15.9	2.3	NORESS
SM3	R1	02/14/86	16:44:08	67.1	20.6	2.6	Helsinki
<i>LENINGRAD MINE EXPLOSIONS</i>							
LM1	V1C	07/25/85	17:32:46	60.9	29.3	2.5	Helsinki
LM2	V1B	12/25/85	14:18:01	60.8	29.3	>2.0	Helsinki

TABLE 4					
SOURCE PARAMETERS FOR PRESUMED EXPLOSIONS IN WESTERN RUSSIA					
EVENT	DATE (m/d/y)	ORIGIN TIME (UTC)	LATITUDE (deg N)	LONGITUDE (deg E)	m_b
E1	07/10/71	16:59:59.3	64.168	55.183	5.3
E2	10/04/71	10:00:02.0	61.613	47.116	5.1
E3	08/14/74	14:59:58.3	68.913	75.899	5.5
E4	08/29/74	14:59:59.6	67.233	62.119	5.2
E5	10/04/79	15:59:57.9	60.677	71.501	5.4
E6	08/11/84	18:59:57.8	65.079	55.287	5.2

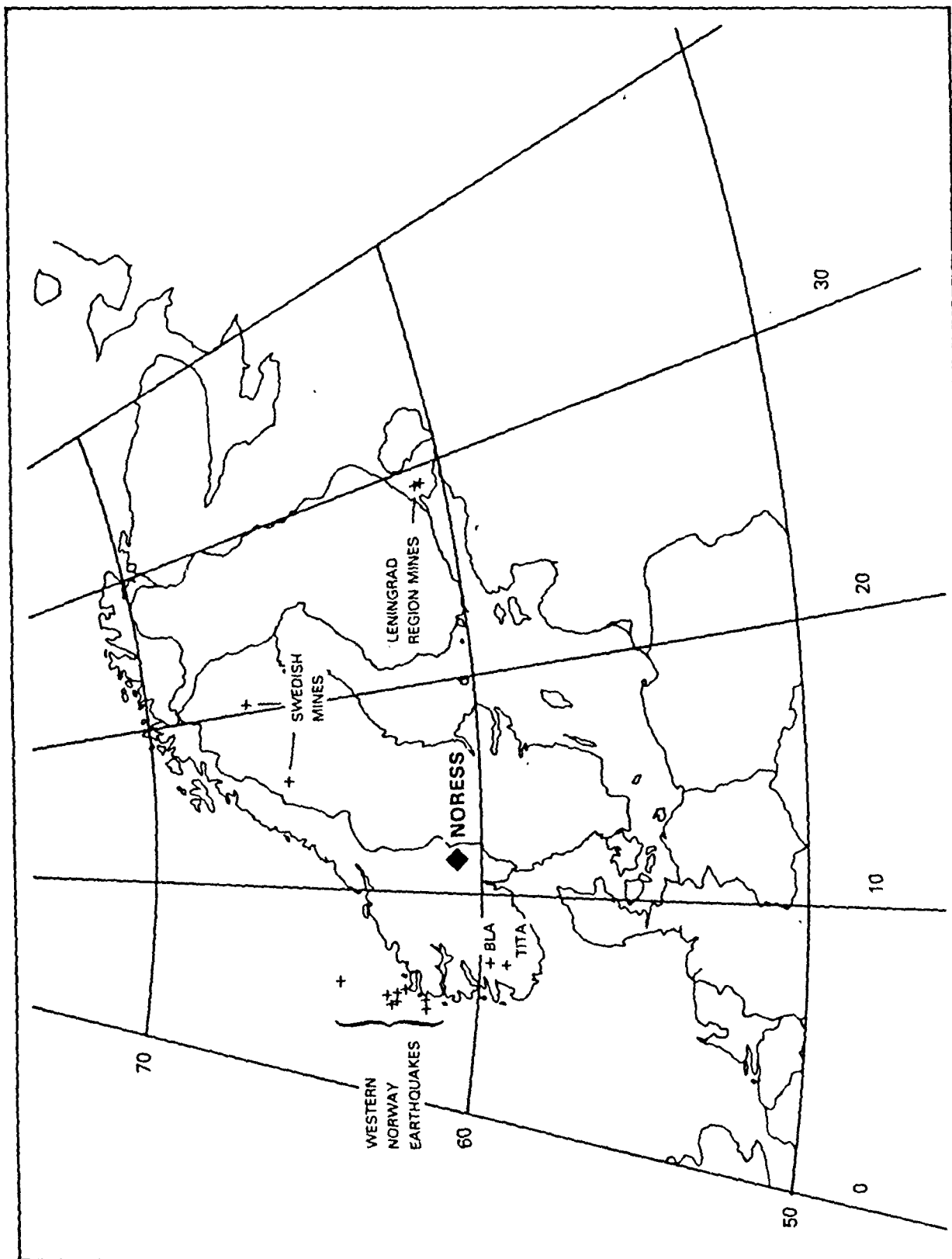


FIGURE 1

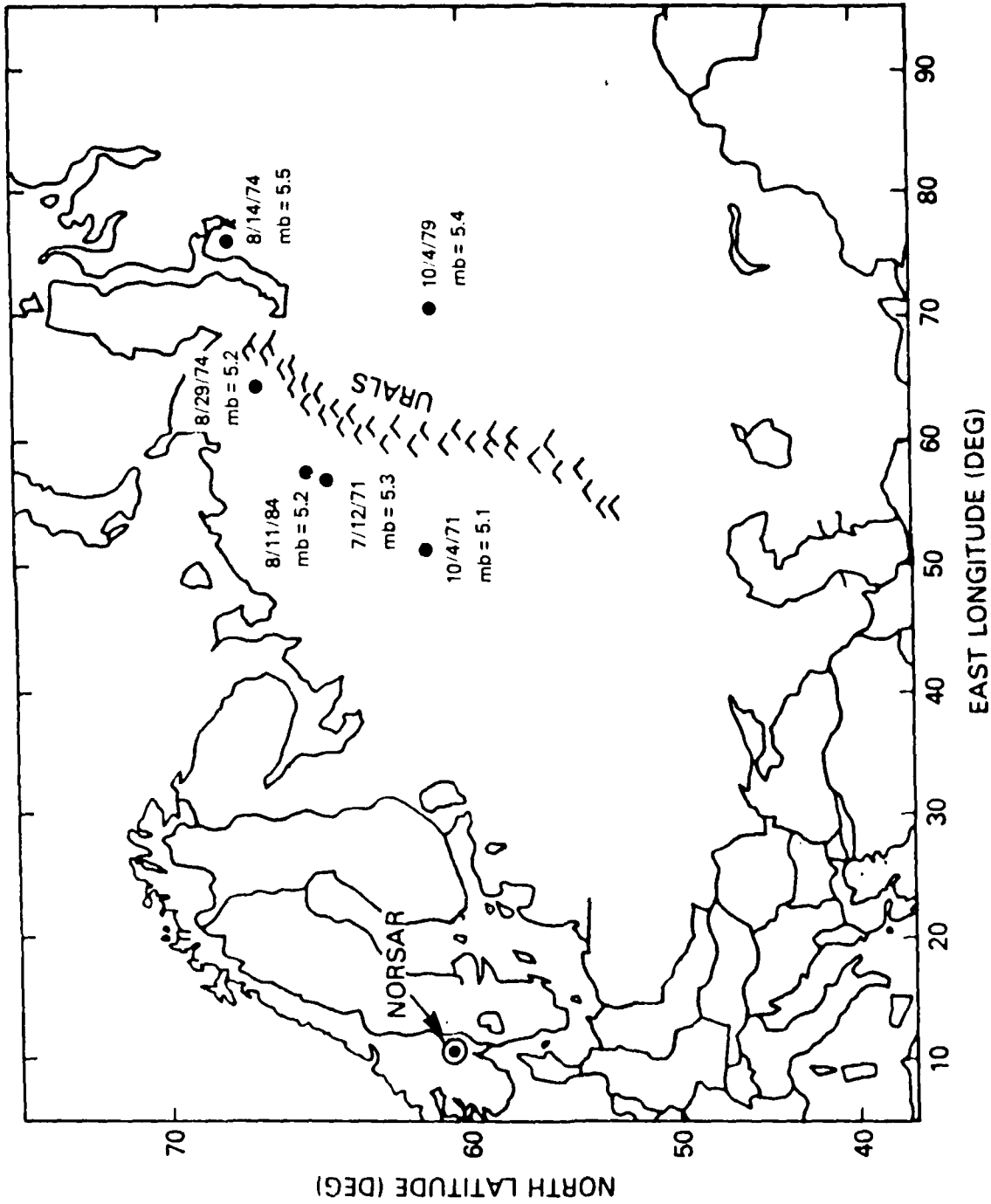


FIGURE 2

WESTERN NORWAY EARTHQUAKE
INCOHERENT BEAMS - ALL FREQUENCIES
O6

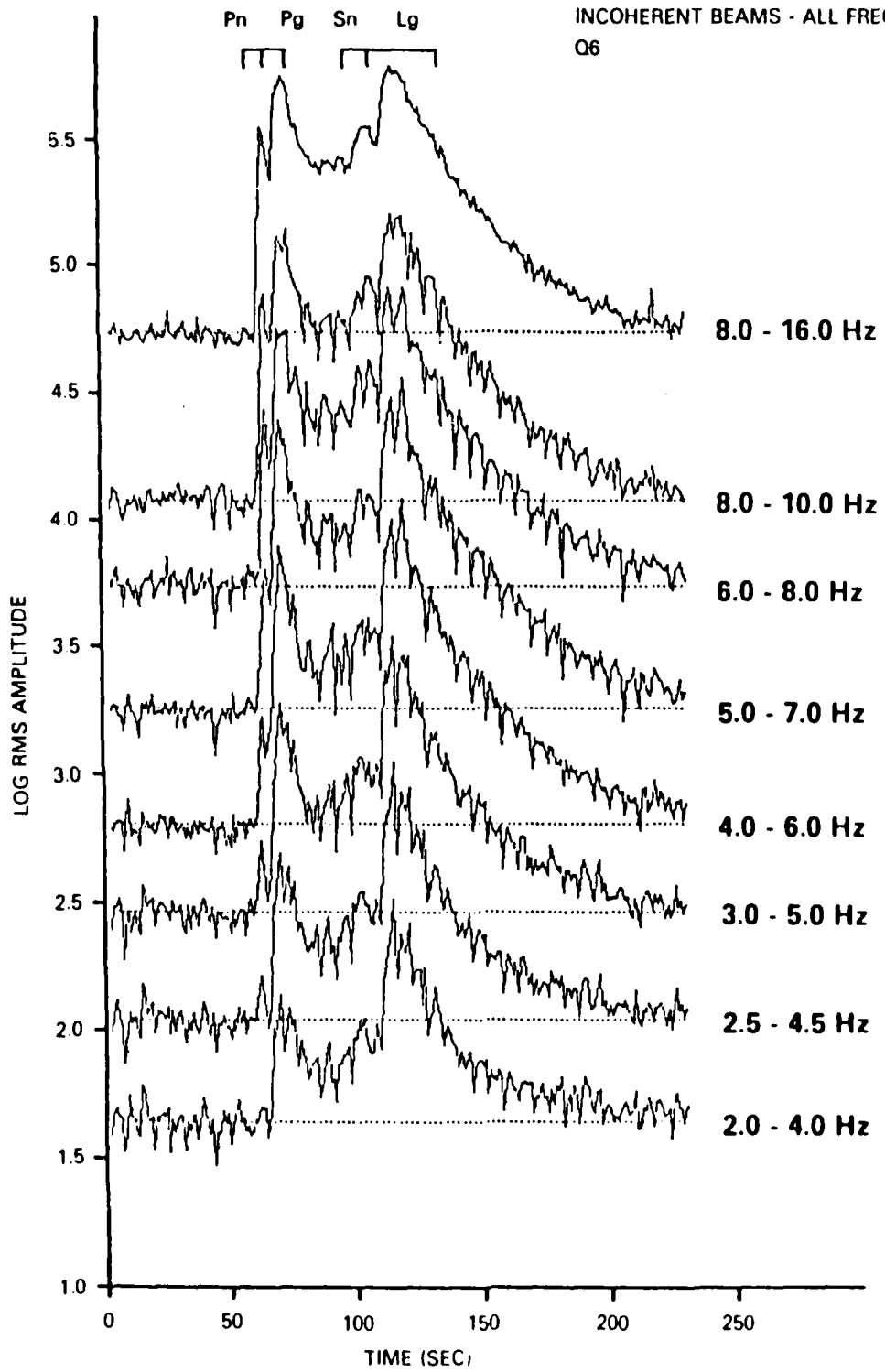


FIGURE 3

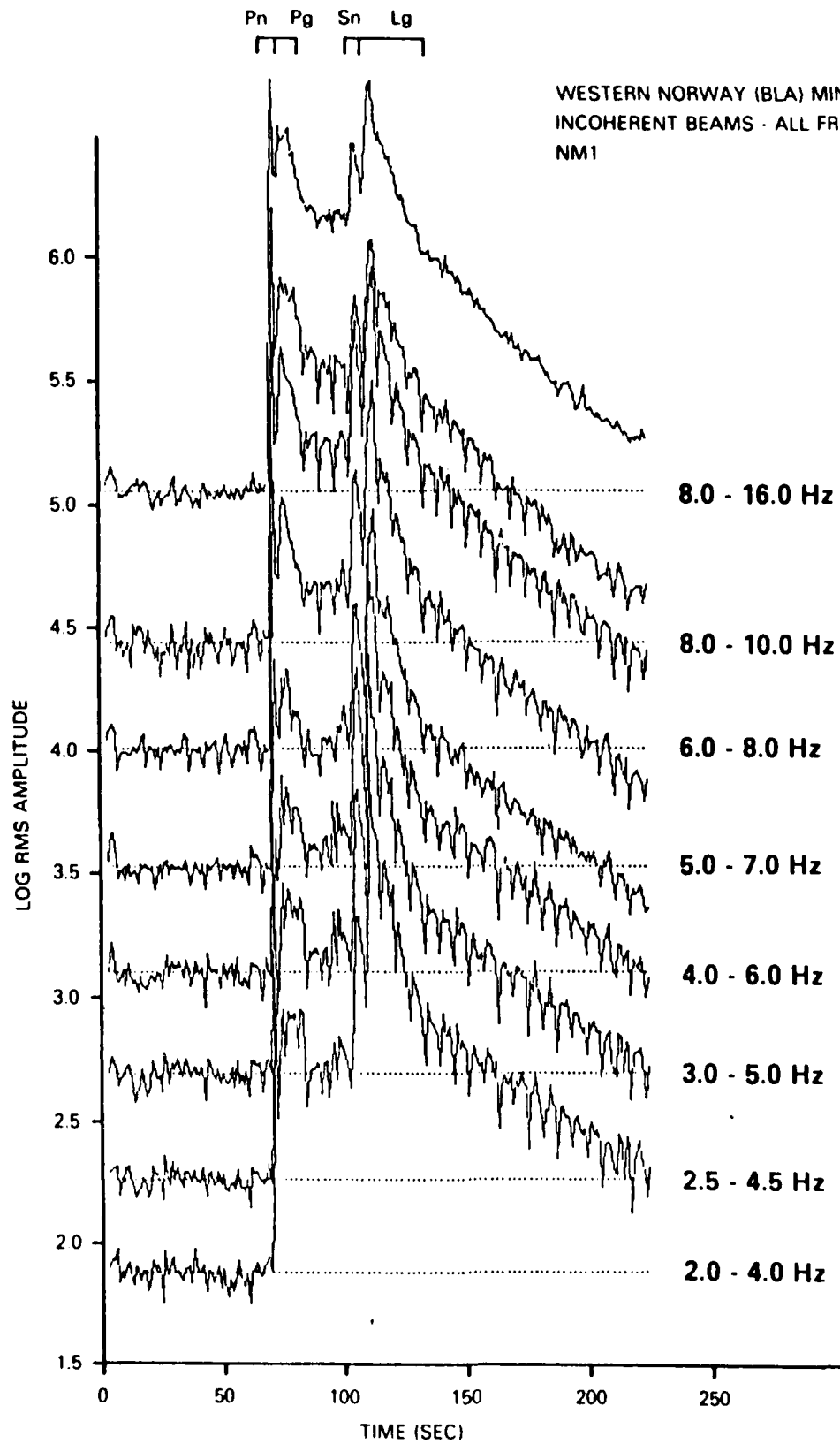


FIGURE 4

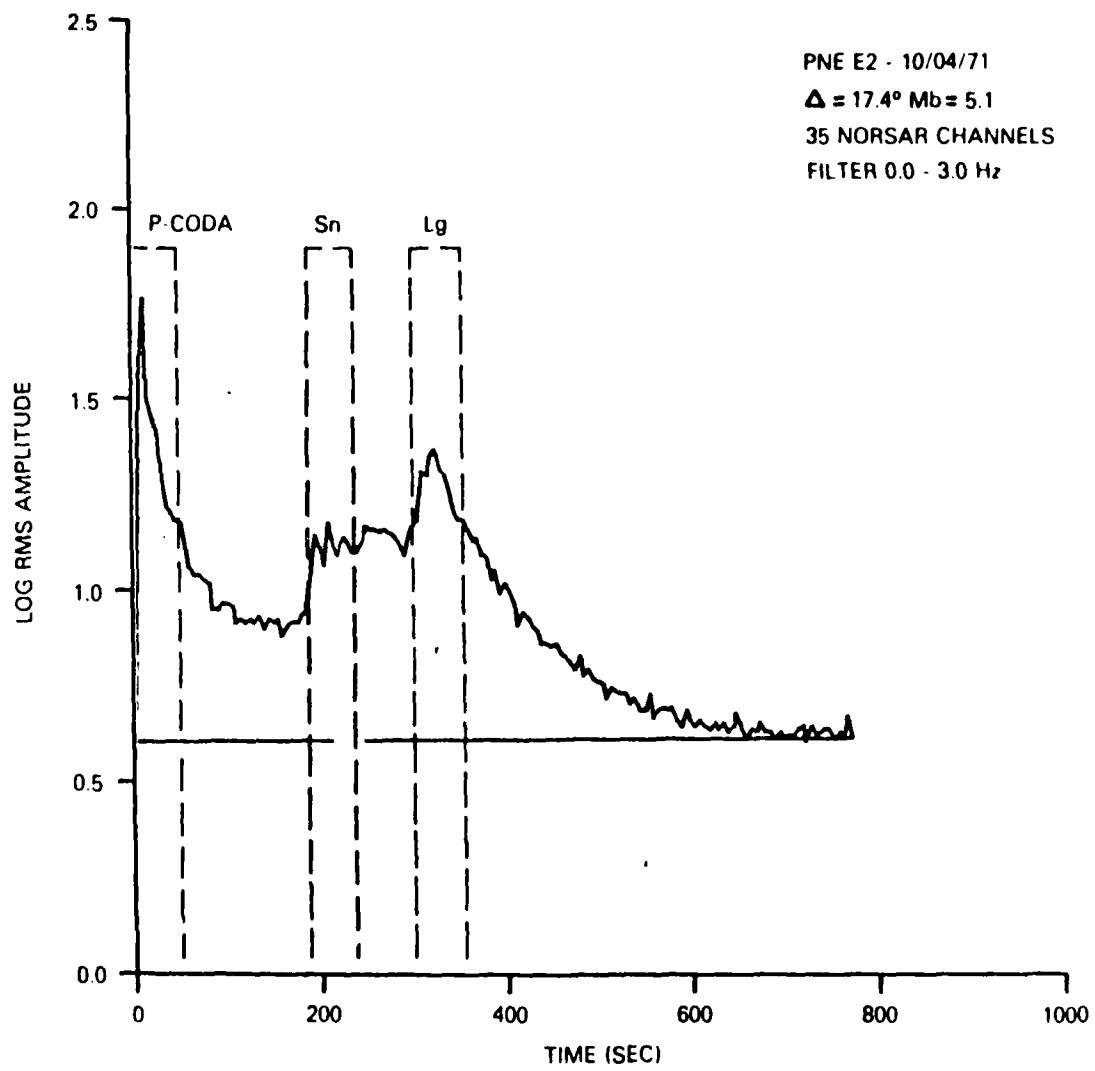


FIGURE 5

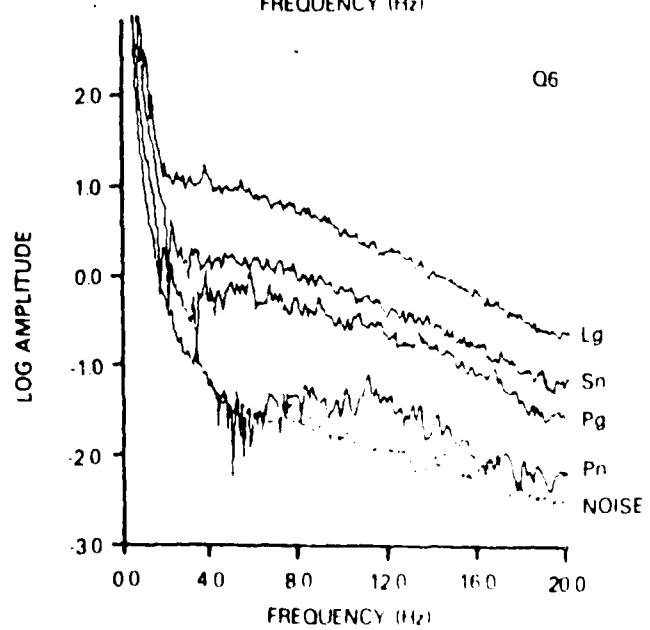
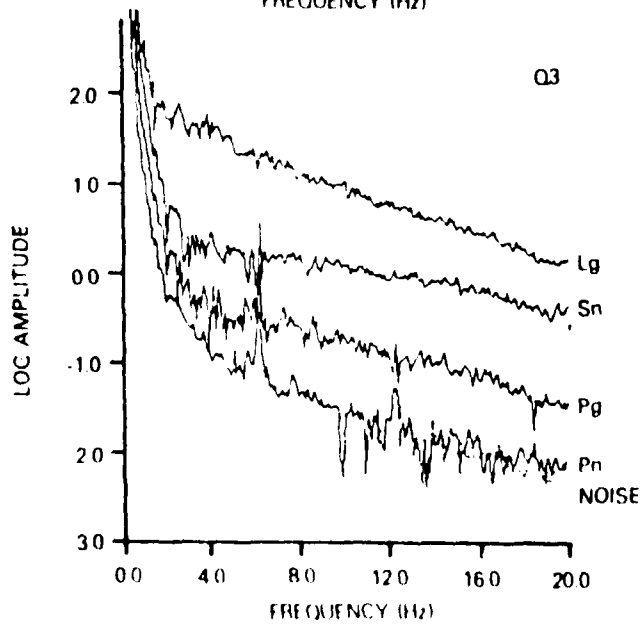
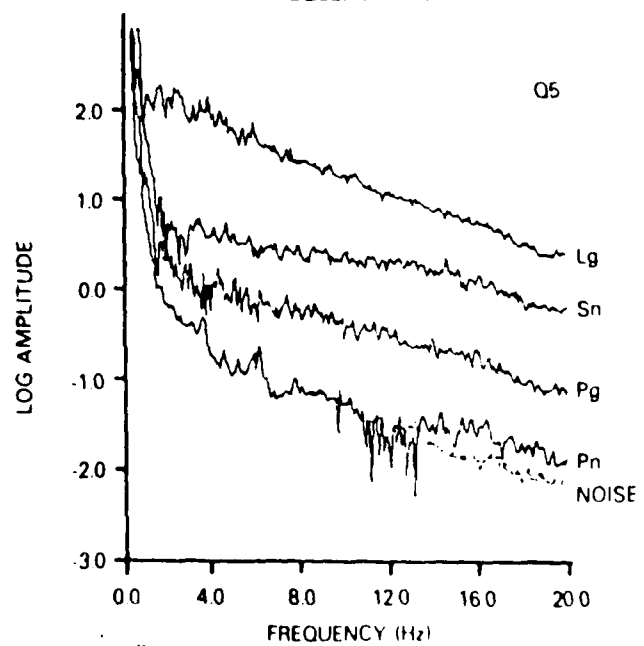
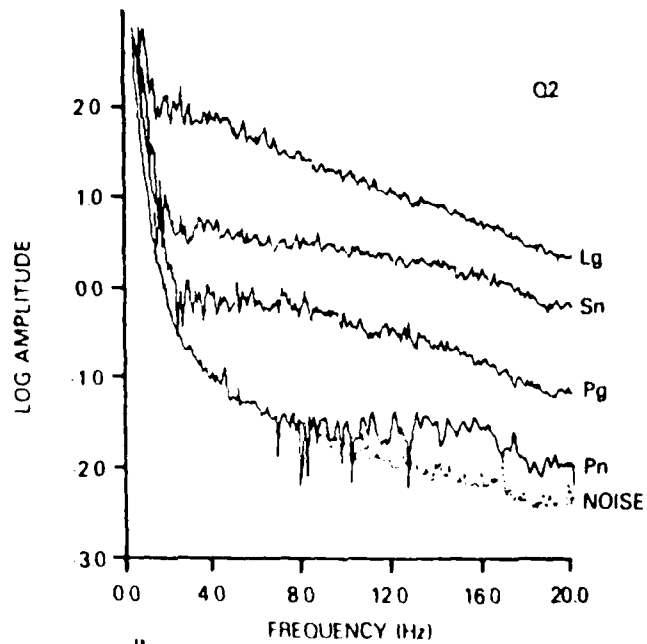
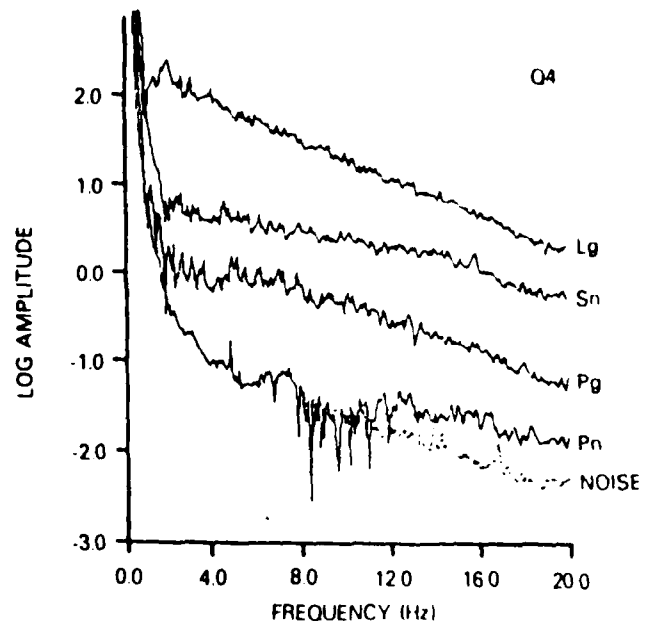
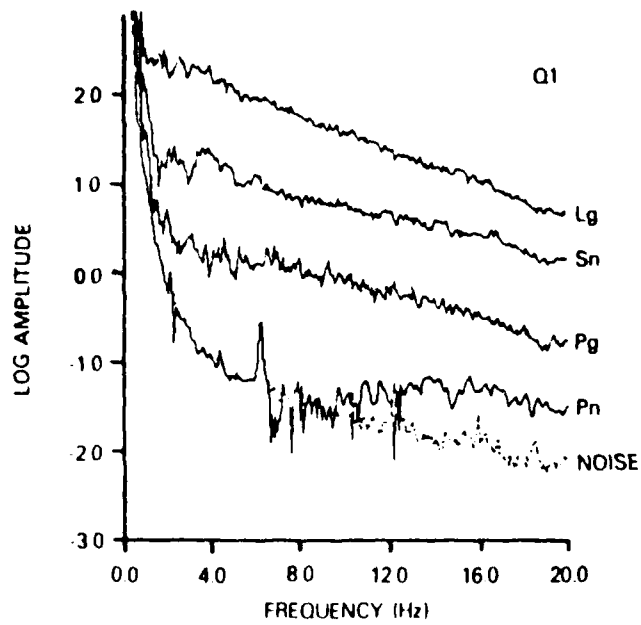


FIGURE 6

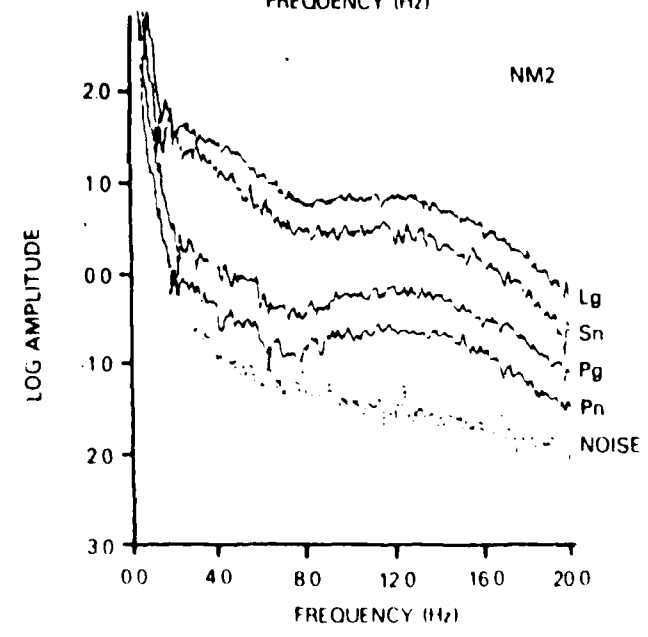
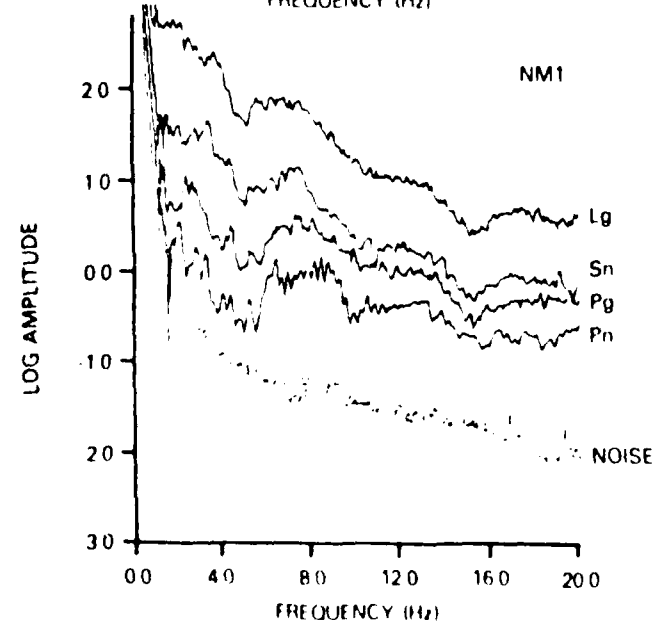
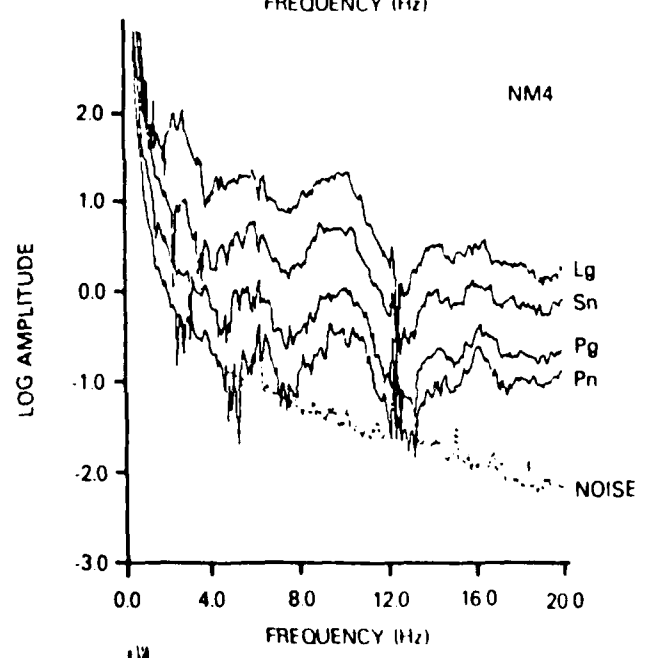
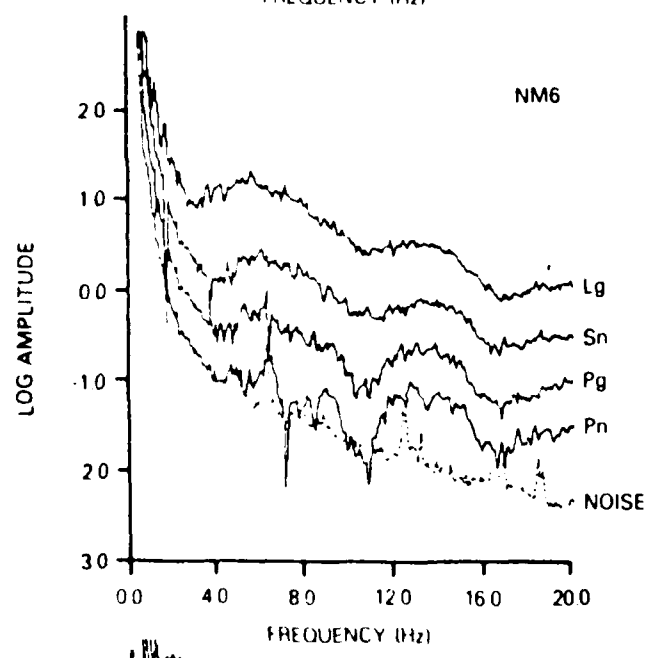
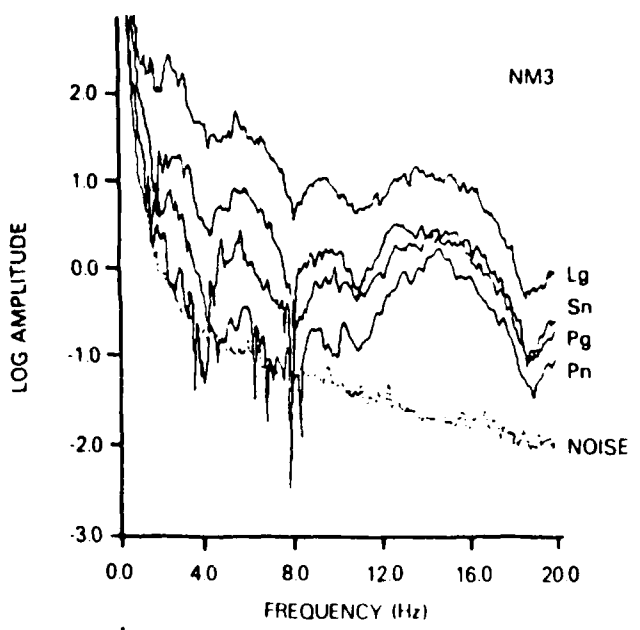
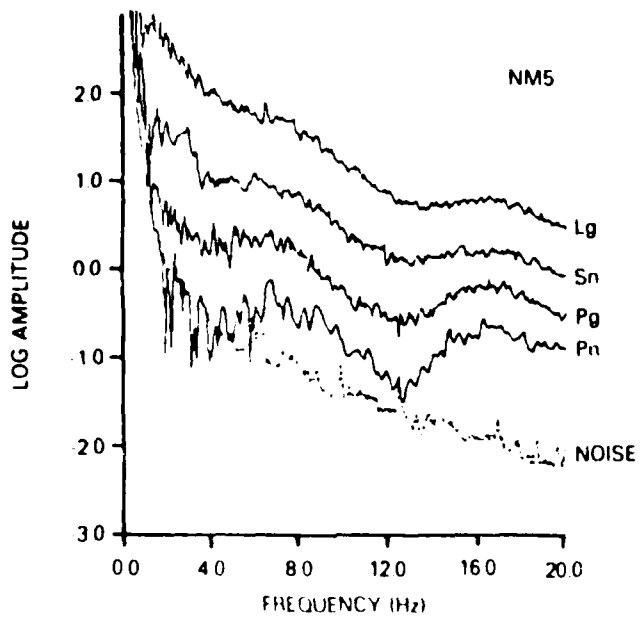


FIGURE 7

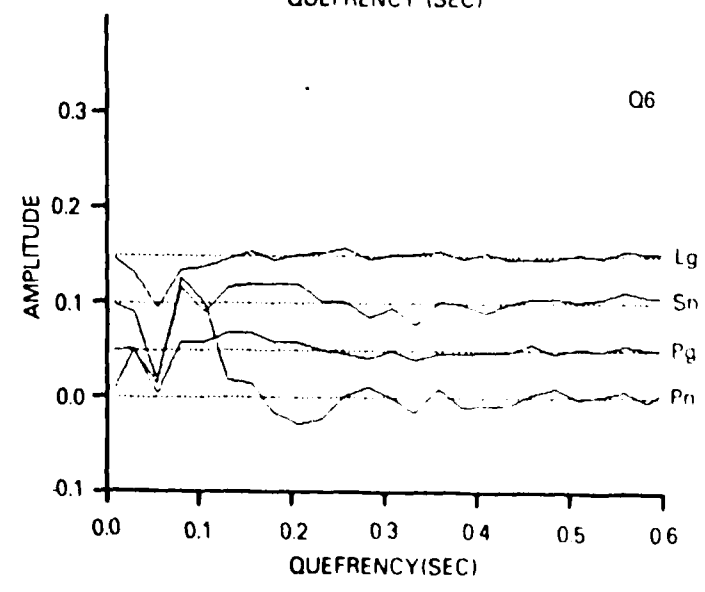
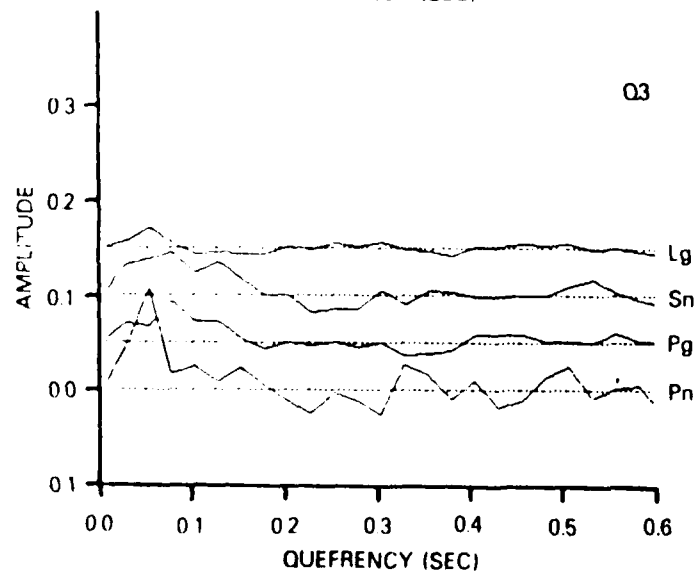
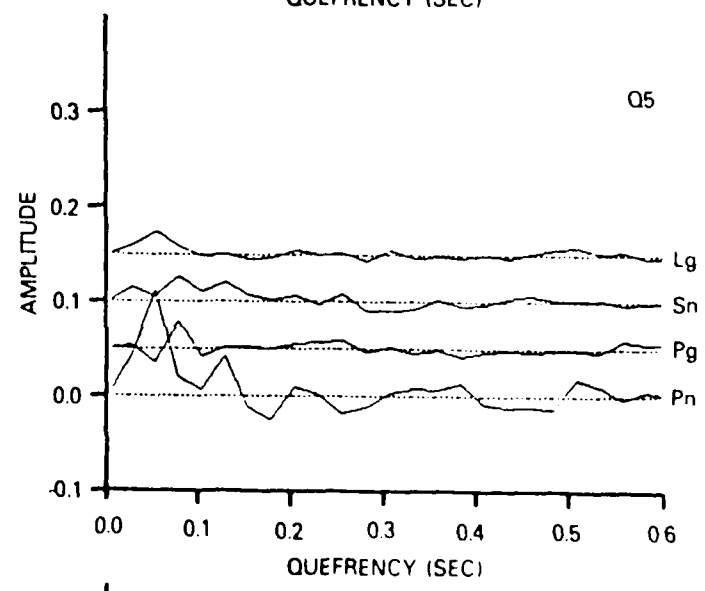
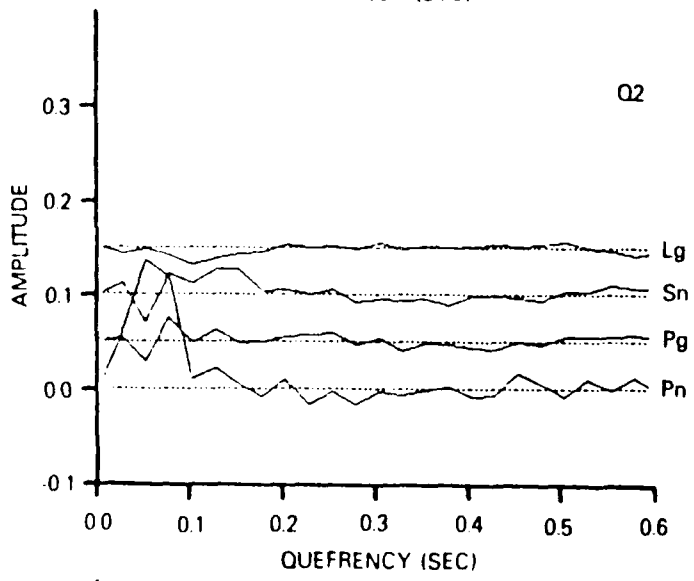
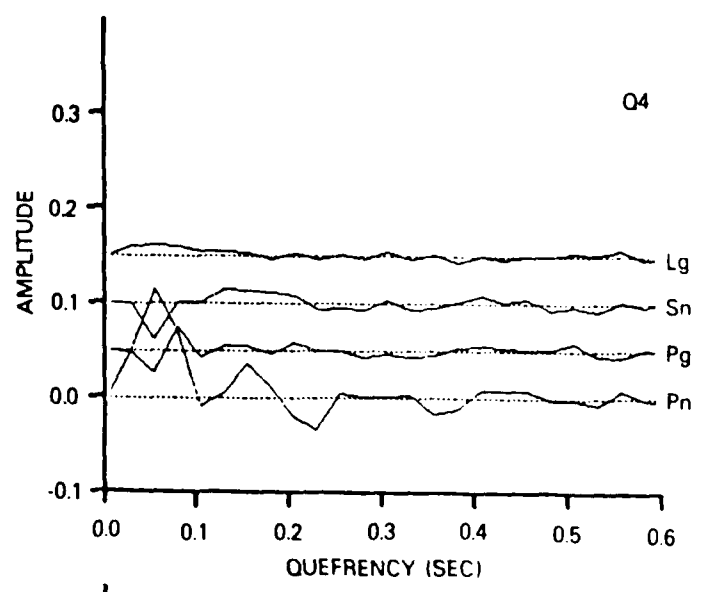
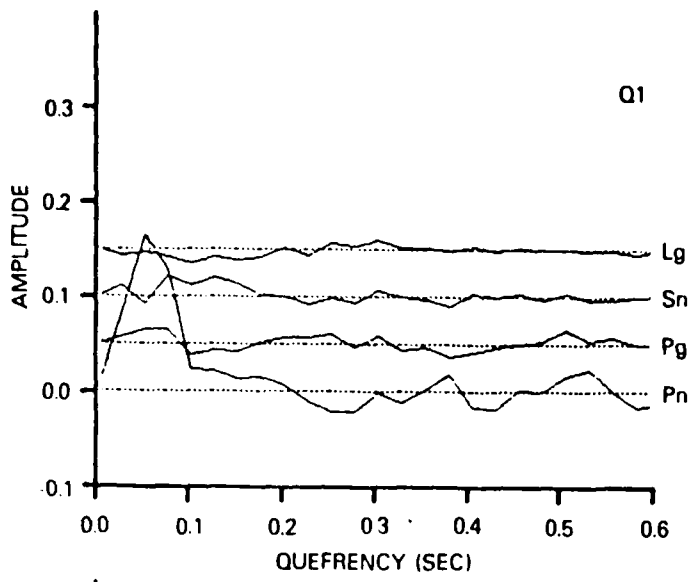


FIGURE 8

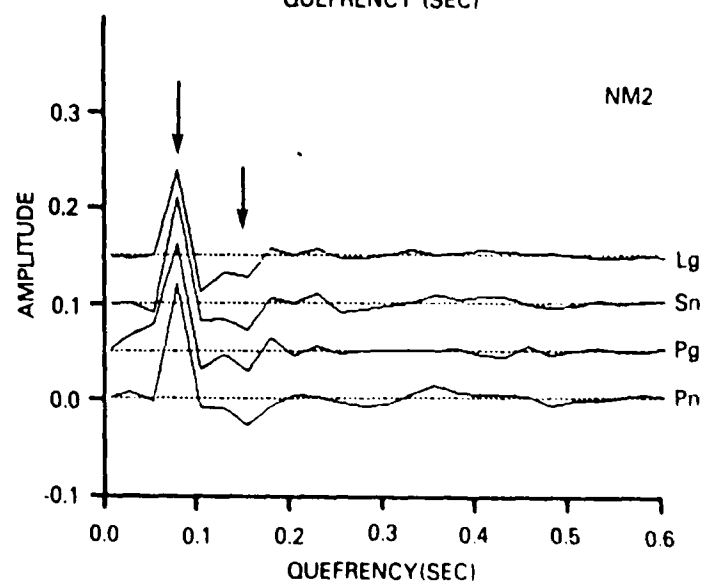
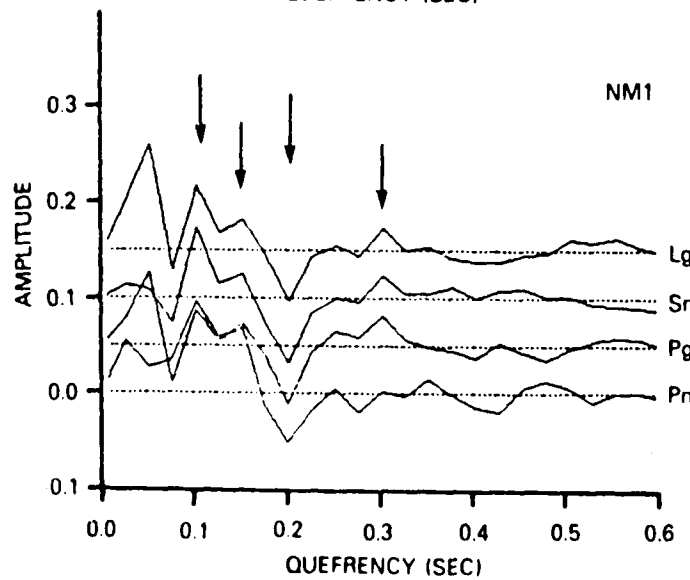
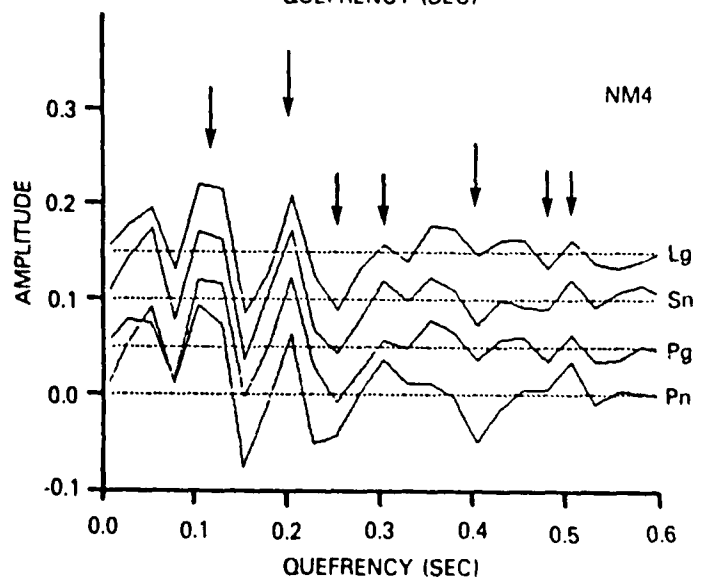
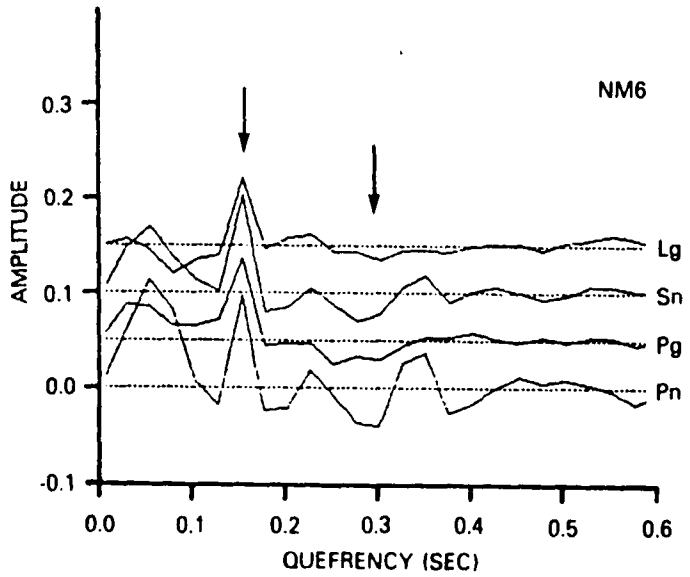
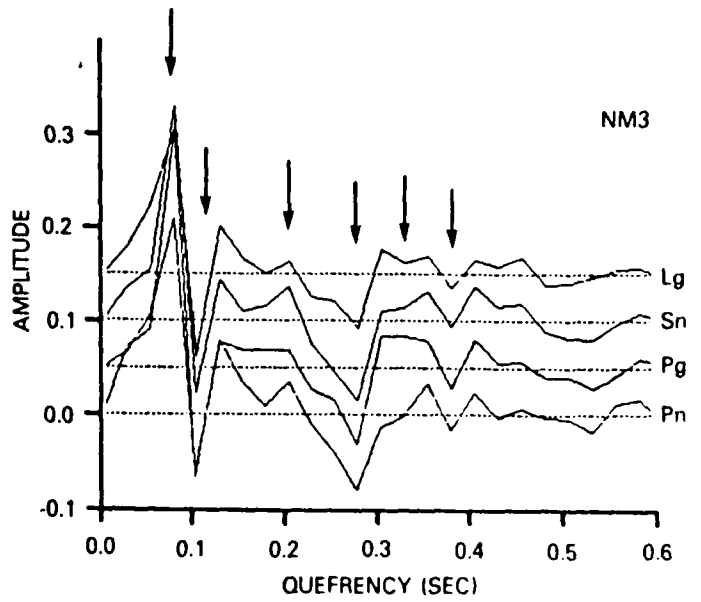
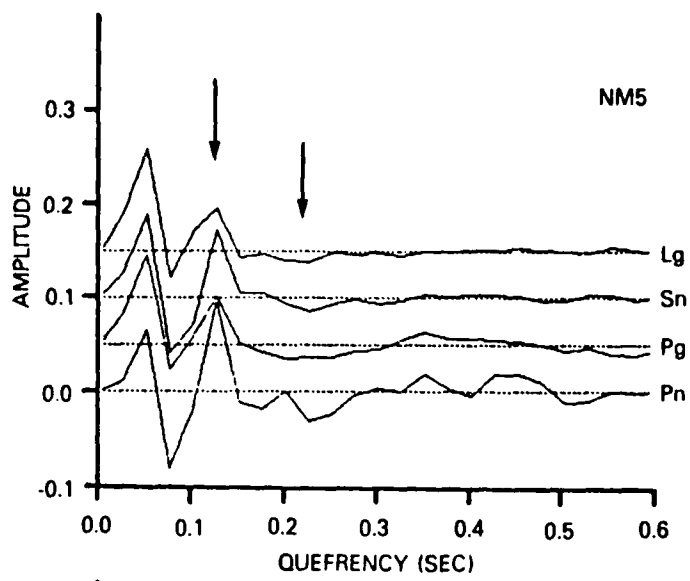


FIGURE 9

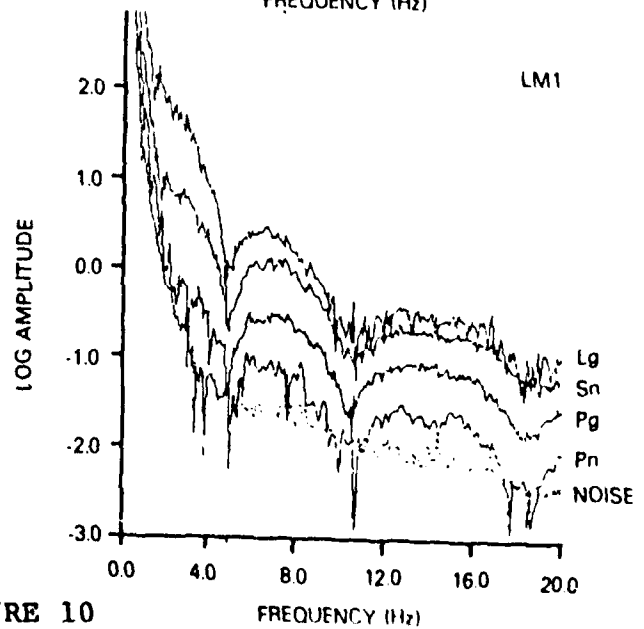
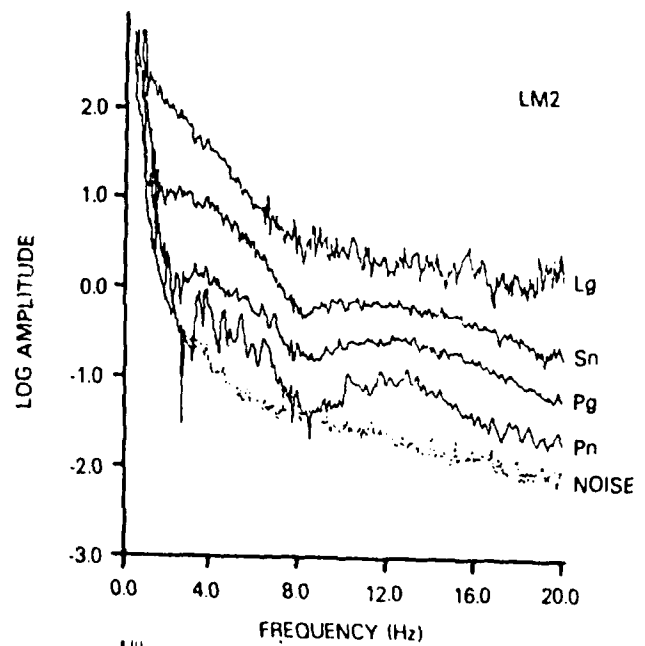
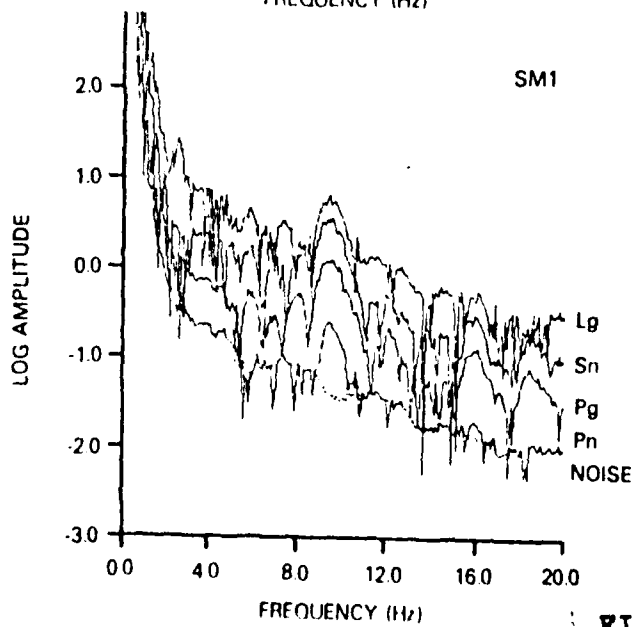
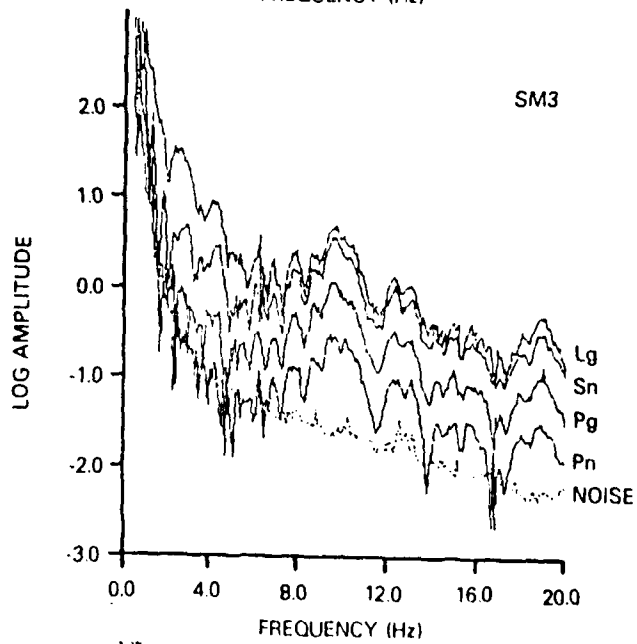
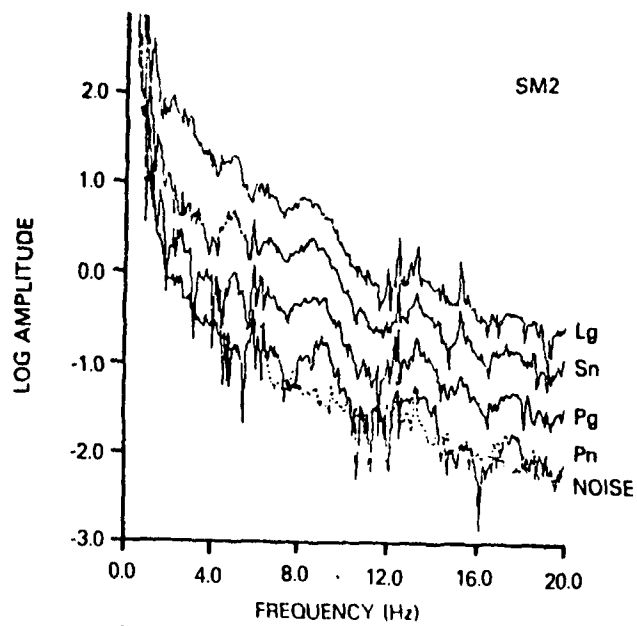


FIGURE 10

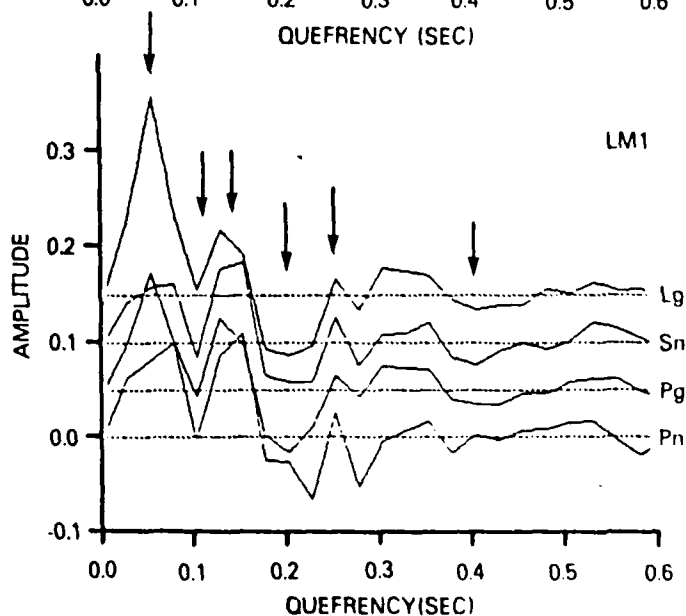
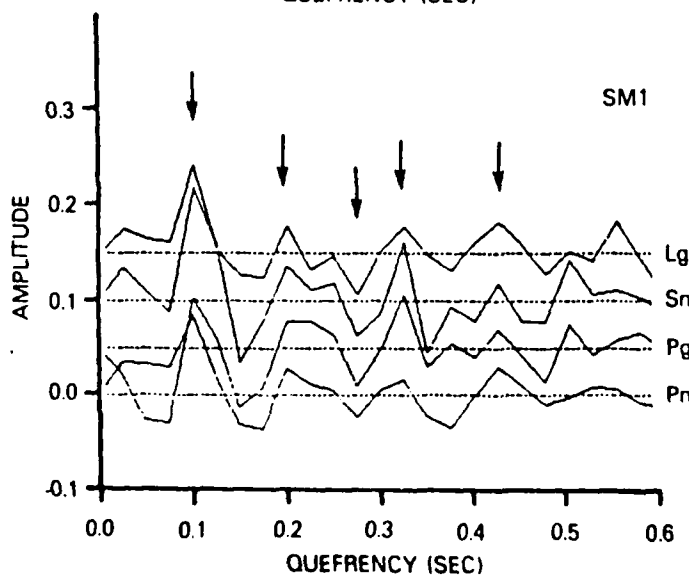
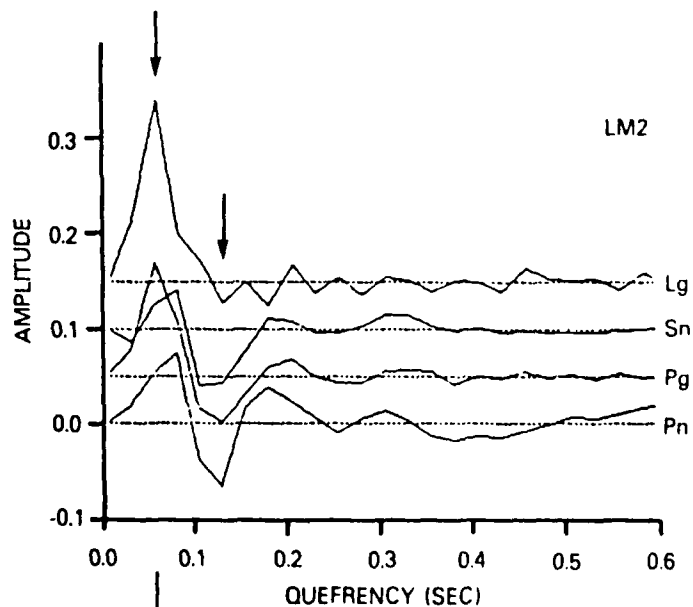
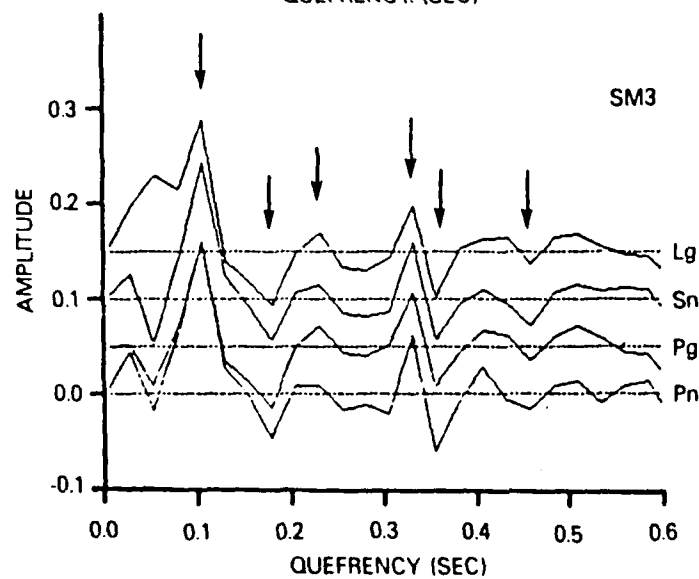
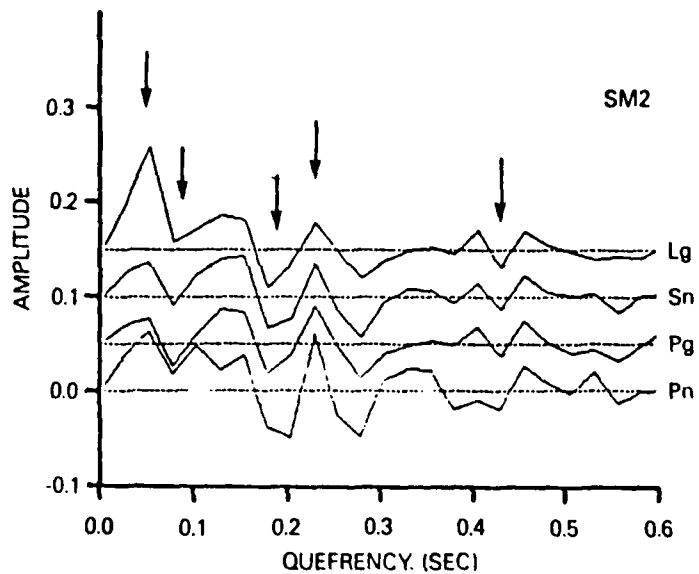


FIGURE 11

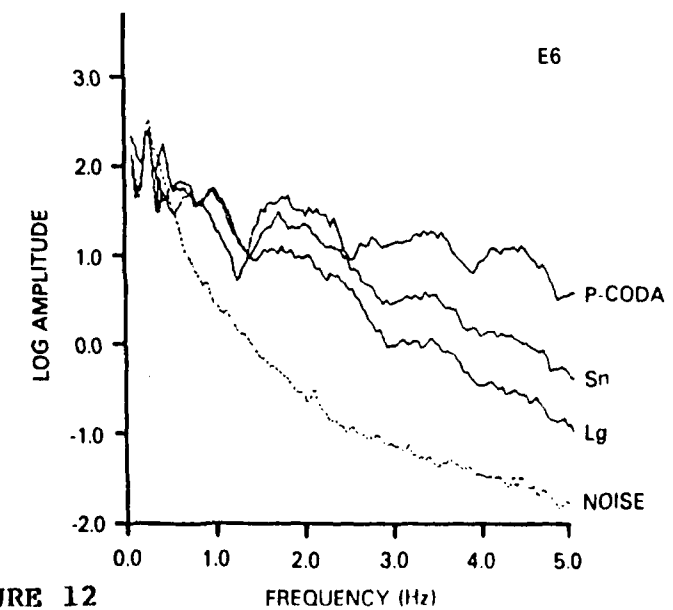
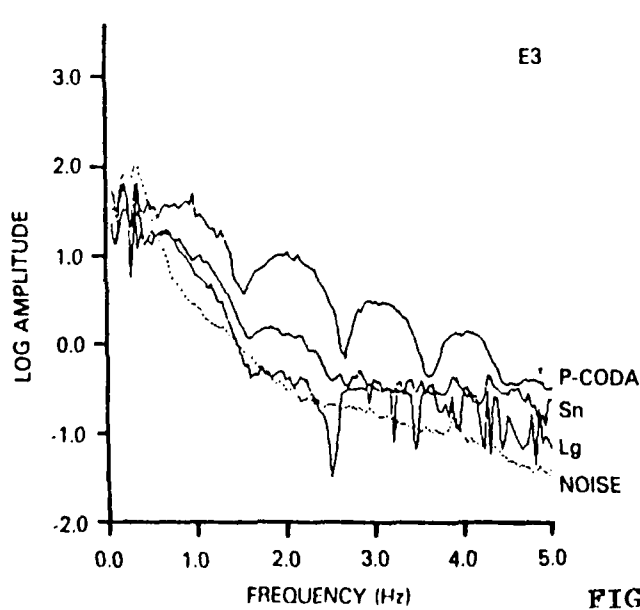
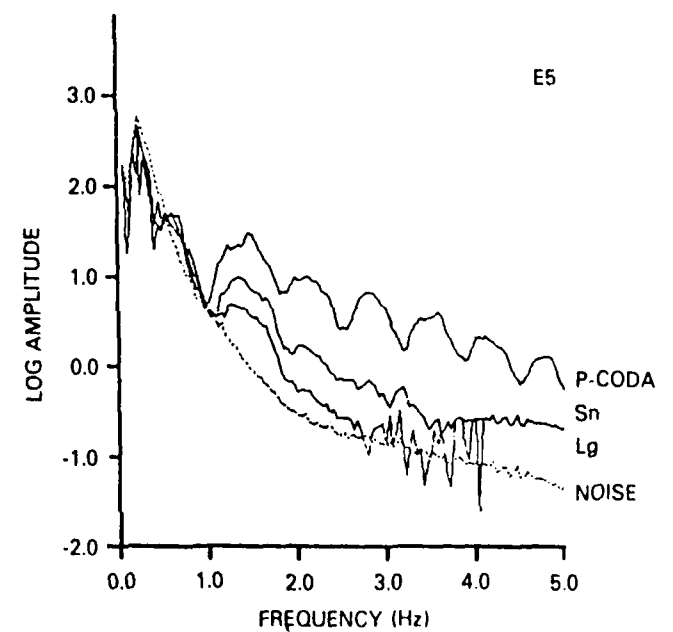
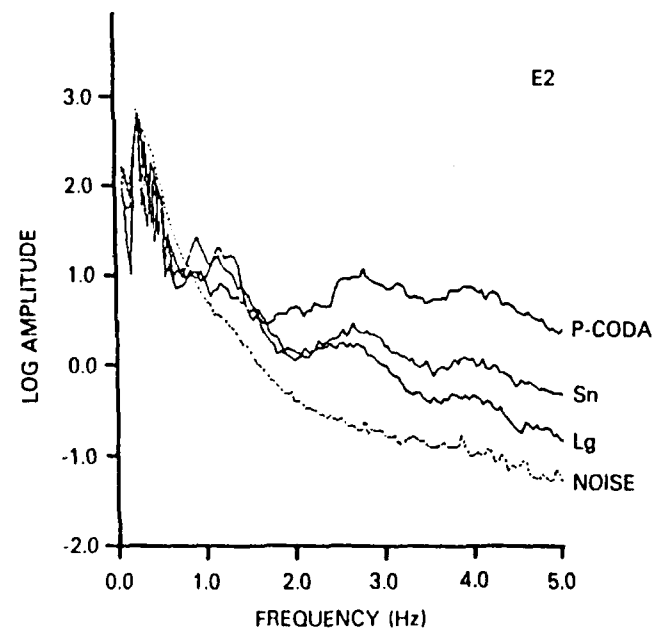
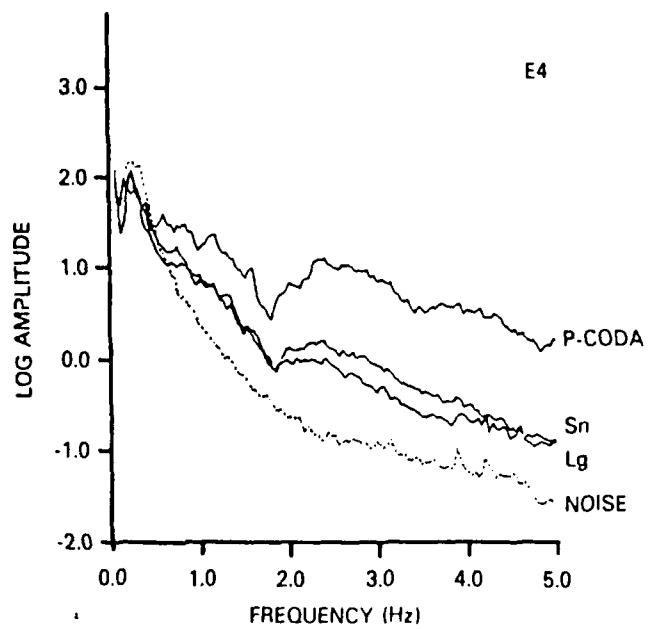
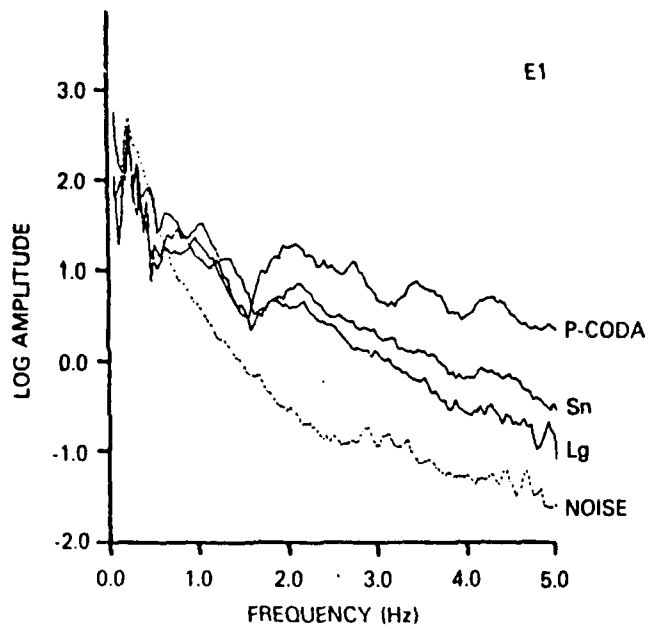


FIGURE 12

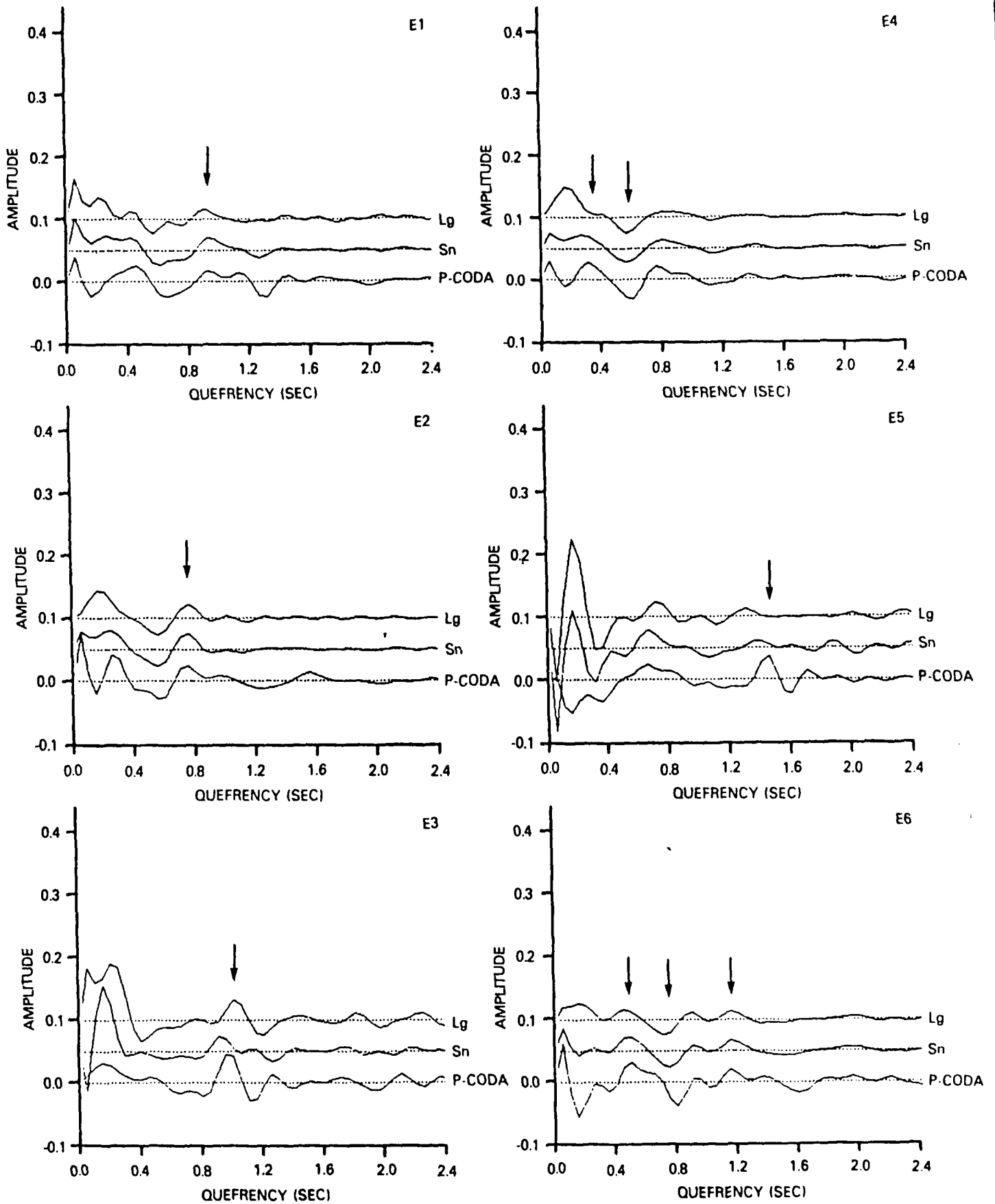
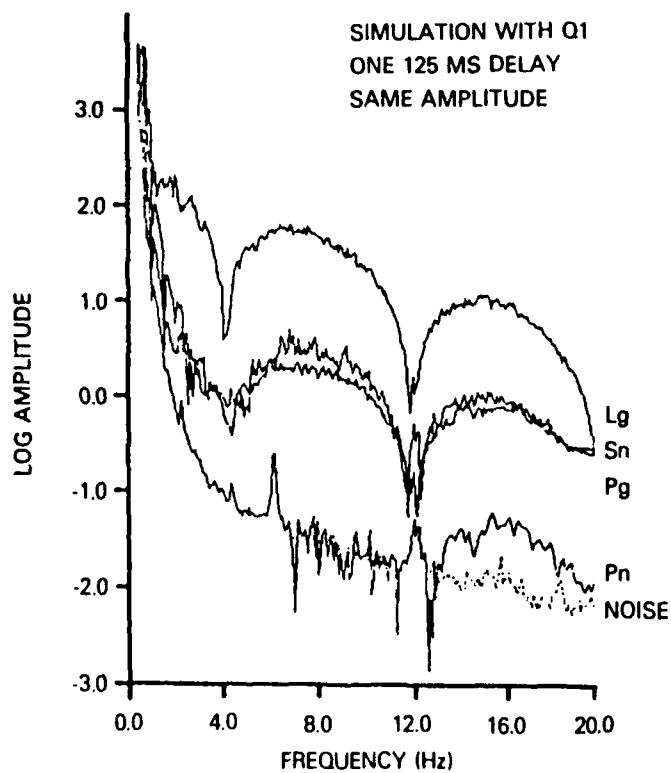
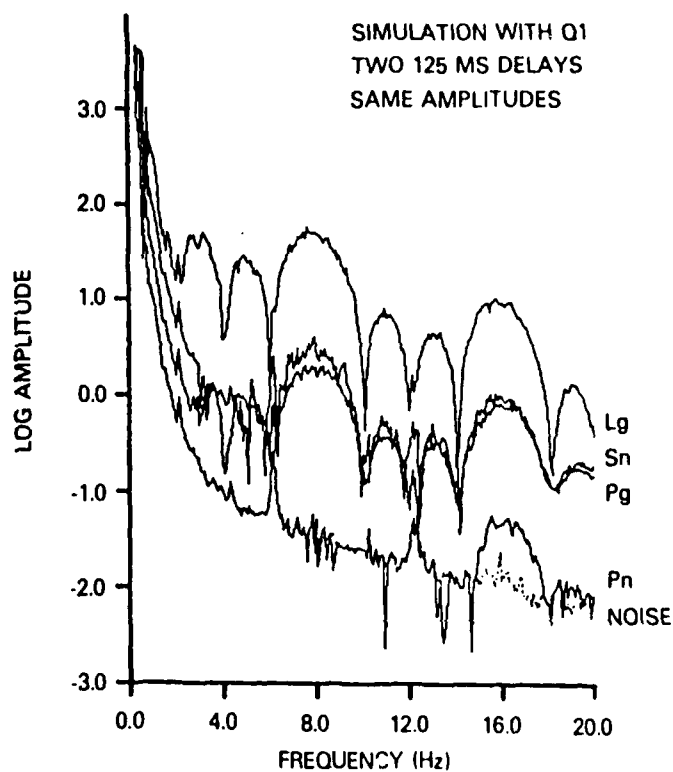


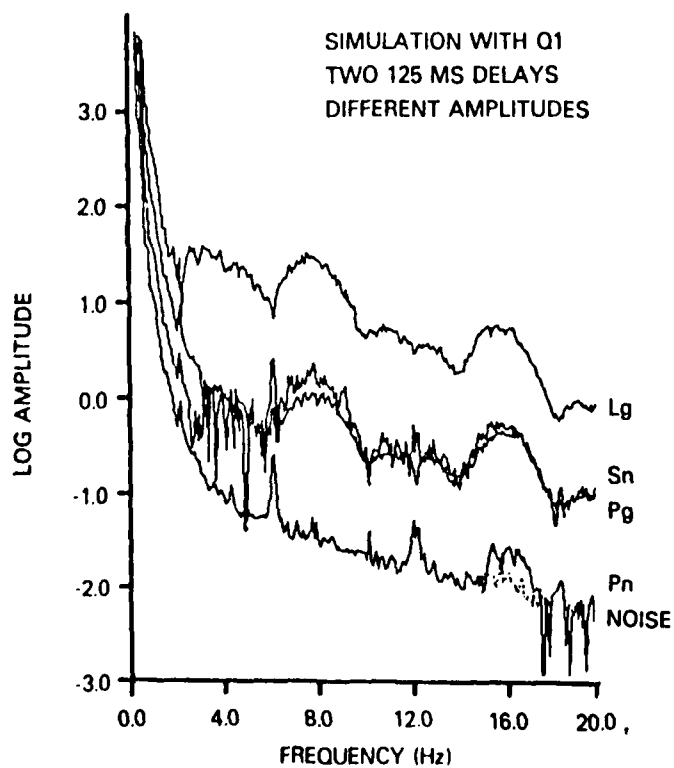
FIGURE 13



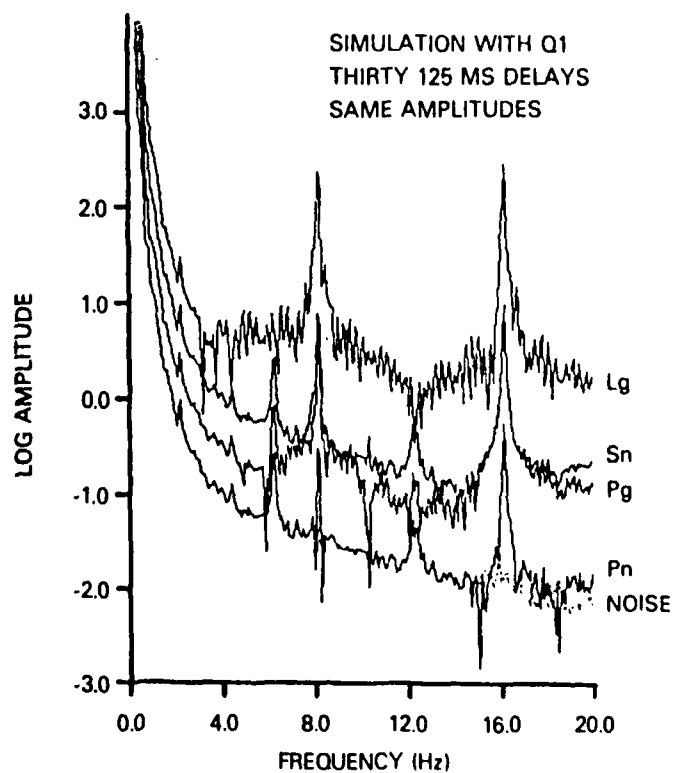
(a)



(b)

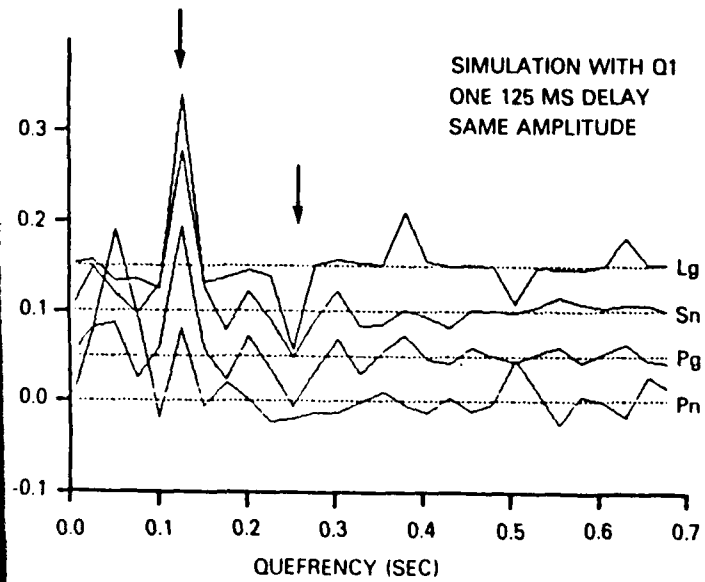


(c)

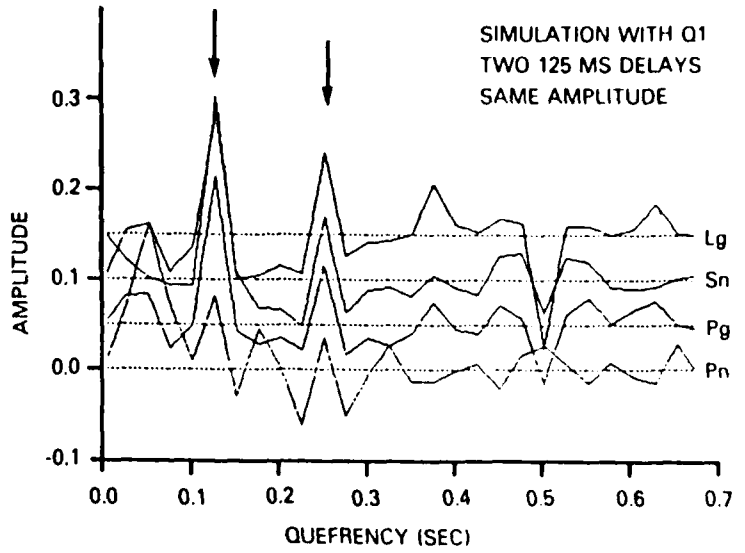


(d)

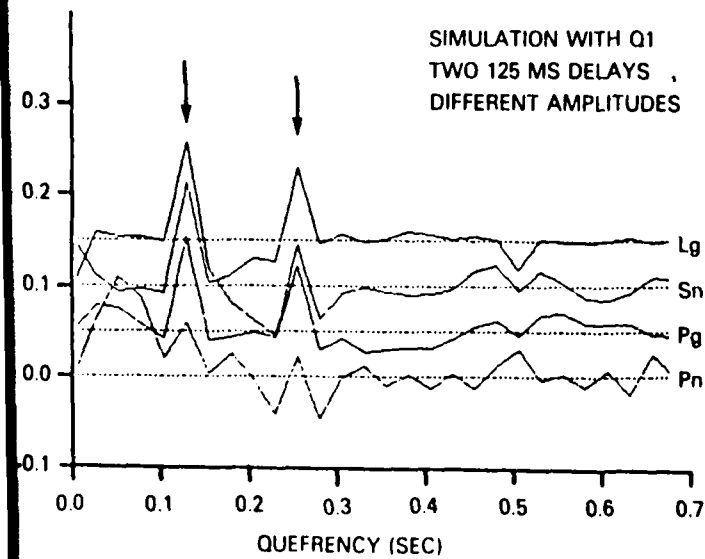
FIGURE 14



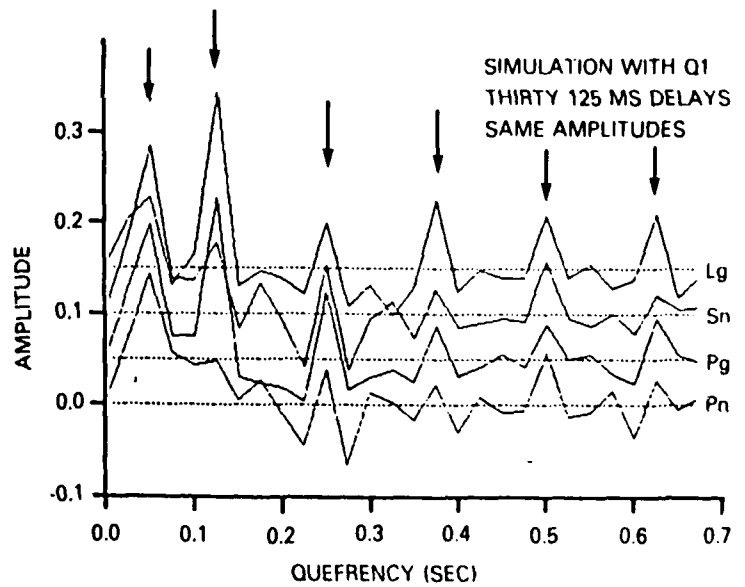
(a)



(b)



(c)



(d)

FIGURE 15

DISTRIBUTION LIST

Dr. Monem Abdel-Gawad
Rockwell International Science Center
1049 Camino Dos Rios
Thousand Oaks, CA 91360

Professor Keiliti Aki
Center for Earth Sciences
University of Southern California
University Park
Los Angeles, CA 90089-0741

Professor Shelton S. Alexander
Geosciences Department
403 Deike Building
The Pennsylvania State University
University Park, PA 16802

Professor Charles B. Archambeau
Cooperative Institute for Research in
Environmental Sciences
University of Colorado
Boulder, CO 80309

Dr. Thomas C. Bache Jr.
Science Applications Int'l Corp.
10210 Campus Point Drive
San Diego, CA 92121

Dr. James Bulau
Rockwell International Science Center
1049 Camino Dos Rios
P.O. Box 1085
Thousand Oaks, CA 91360

Dr. Douglas R. Baumgardt
Signal Analysis and Systems Division
ENSCO, Inc.
5400 Port Royal Road
Springfield, VA 22151-2388

Dr. S. Bratt
Science Applications Int'l Corp.
10210 Campus Point Drive
San Diego, CA 92121

Professor John Ebel
Department of Geology & Geophysics
Boston College
Chestnut Hill, MA 02167

Woodward-Clyde Consultants
Attn: Dr. Lawrence J. Burdick
Dr. Jeff Barker
P.O. Box 93245
Pasadena, CA 91109-3245 (2 copies)

Dr. Roy Burger
1221 Serry Rd.
Schenectady, NY 12309

Professor Robert W. Clayton
Seismological Laboratory
Division of Geological and Planetary
Sciences
California Institute of Technology
Pasadena, CA 91125

Dr. Vernon F. Cormier
Earth Resources Laboratory
Department of Earth, Atmospheric and
Planetary Sciences
Massachusetts Institute of Technology
42 Carleton Street
Cambridge, MA 02142

Professor Anton M. Dainty
Earth Resources Laboratory
Department of Earth, Atmospheric and
Planetary Sciences
Massachusetts Institute of Technology
42 Carleton Street
Cambridge, MA 02142

Dr. Zoltan A. Der
Teledyne Geotech
314 Montgomery Street
Alexandria, VA 22314

Prof. Adam Dziewonski
Hoffman Laboratory
Harvard University
20 Oxford St.
Cambridge, MA 02138

Professor John Ferguson
Center for Lithospheric Studies
The University of Texas at Dallas
P.O. Box 830688
Richardson, TX 75083-0688

Dr. Jeffrey W. Given
Sierra Geophysics
11255 Kirkland Way
Kirkland, WA 98033

Professor Charles A. Langston
Geosciences Department
403 Deike Building
The Pennsylvania State University
University Park, PA 16802

Prof. Roy Greenfield
Geosciences Department
403 Deike Building
The Pennsylvania State University
University Park, PA 16802

Professor Thorne Lay
Department of Geological Sciences
1006 C.C. Little Building
University of Michigan
Ann Arbor, MI 48109-1063

Professor David G. Harkrider
Seismological Laboratory
Division of Geological and Planetary
Sciences
California Institute of Technology
Pasadena, CA 91125

Dr. George R. Mellman
Sierra Geophysics
11255 Kirkland Way
Kirkland, WA 98033

Professor Donald V. HelMBERGER
Seismological Laboratory
Division of Geological and Planetary
Sciences
California Institute of Technology
Pasadena, CA 91125

Professor Brian J. Mitchell
Department of Earth and Atmospheric
Sciences
Saint Louis University
Saint Louis, MO 63156

Professor Eugene Herrin
Institute for the Study of Earth & Man
Geophysical Laboratory
Southern Methodist University
Dallas, TX 75275

Professor Thomas V. McEvilly
Seismographic Station
University of California
Berkeley, CA 94720

Professor Robert B. Herrmann
Department of Earth and Atmospheric
Sciences
Saint Louis University
Saint Louis, MO 63156

Dr. Keith L. McLaughlin
Teledyne Geotech
314 Montgomery Street
Alexandria, VA 22314

Professor Lane R. Johnson
Seismographic Station
University of California
Berkeley, CA 94720

Professor Otto W. Nuttli
Department of Earth and Atmospheric
Sciences
Saint Louis University
Saint Louis, MO 63156

Professor Thomas H. Jordan
Department of Earth, Atmospheric and
Planetary Sciences
Massachusetts Institute of Technology
Cambridge, MA 02139

Professor Paul G. Richards
Lamont-Doherty Geological Observatory
of Columbia University
Palisades, NY 10964

Dr. Alan Kafka
Department of Geology & Geophysics
Boston College
Chestnut Hill, MA 02167

Dr. Norton Rimer
S-Cubed
A Division of Maxwell Laboratory
P.O. 1620
La Jolla, CA 92038-1620

Professor Larry J. Ruff
Department of Geological Sciences
1006 C.C. Little Building
University of Michigan
Ann Arbor, MI 48109-1063

Professor Charles G. Sammis
Center for Earth Sciences
University of Southern California
University Park
Los Angeles, CA 90089-0741

Dr. David G. Simpson
Lamont-Doherty Geological Observatory
of Columbia University
Palisades, NY 10964

Dr. Jeffrey L. Stevens
S-CUBED,
A Division of Maxwell Laboratory
P.O. Box 1620
La Jolla, CA 92038-1620

Professor Brian Stump
Institute for the Study of Earth
and Man
Geophysical Laboratory
Southern Methodist University
Dallas, TX 75275

Professor Ta-liang Teng
Center for Earth Sciences
University of Southern California
University Park
Los Angeles, CA 90089-0741

Dr. R. B. Tittmann
Rockwell International Science Center
1049 Camino Dos Rios
P.O. Box 1085
Thousand Oaks, CA 91360

Professor M. Nafi Toksoz
Earth Resources Laboratory
Department of Earth, Atmospheric and
Planetary Sciences
Massachusetts Institute of Technology
42 Carleton Street
Cambridge, MA 02142

Professor Terry C. Wallace
Department of Geosciences
Building #11
University of Arizona
Tucson, AZ 85721

Prof. John H. Woodhouse
Hoffman Laboratory
Harvard University
20 Oxford St.
Cambridge, MA 02138

Dr. G. Blake
US Dept of Energy/DP 331
Forrestal Building
1000 Independence Ave.
Washington, D.C. 20585

Dr. Michel Bouchon
Universite Scientifique et
Medicale de Grenoble
Laboratoire de Geophysique
Interne et Tectonophysique
I.R.I.G.M.-B.P. 68
38402 St. Martin D'Herès
Cedex FRANCE

Dr. Hilmar Bungum
NTNF/NORSAR
P.O. Box 51
Norwegian Council of Science,
Industry and Research, NORSAR
N-2007 Kjeller, NORWAY

Dr. Alan Douglas
Ministry of Defense
Blacknest, Brimpton, Reading RG7-4RS
UNITED KINGDOM

Professor Peter Harjes
Institute for Geophysik
Rhur University
Bochum
P.O. Box 102148
4630 Bochum 1
FEDERAL REPUBLIC OF GERMANY

Dr. James Hannon
Lawrence Livermore National Laboratory
P.O. Box 808
Livermore, CA 94550

Dr. E. Husebye
NTNF/NORSAR
P.O. Box 51
N-2007 Kjeller, NORWAY

Dr. Arthur Lerner-Lam
Lamont-Doherty Geological Observatory
of Columbia University
Palisades, NY 10964

Mr. Peter Marshall
Procurement Executive
Ministry of Defense
Blacknest, Brimpton, Reading RG7-4RS
UNITED KINGDOM

Dr. B. Massinon
Societe Radiomana
27, Rue Claude Bernard
75005, Paris, FRANCE

Dr. Pierre Mechler
Societe Radiomana
27, Rue Claude Bernard
75005, Paris, FRANCE

Mr. Jack Murphy
S-CUBED
Reston Geophysics Office
11800 Sunrise Valley Drive
Suite 1212
Reston, VA 22091

Dr. Svein Mykkeltveit
NTNF/NORSAR
P.O. Box 51
N-2007 Kjeller, NORWAY

Dr. Carl Newton
Los Alamos National Laboratory
P.O. Box 1663
Mail Stop C 335, Group ESS3
Los Alamos, NM 87545

Dr. Peter Basham
Earth Physics Branch
Department of Energy and Mines
1 Observatory Crescent
Ottawa, Ontario
CANADA K1A 0Y3

Professor J. A. Orcutt
Geological Sciences Division
Univ. of California at San Diego
La Jolla, CA 92093

Dr. Frank F. Pilotte
Director of Geophysics
Headquarters Air Force Technical
Applications Center
Patrick AFB, Florida 32925-6001

Professor Keith Priestley
University of Nevada
Mackay School of Mines
Reno, Nevada 89557

Mr. Jack Raclin
USGS - Geology, Rm 3C136
Mail Stop 928 National Center
Reston, VA 22092

Dr. Frode Ringdal
NTNF/NORSAR
P.O. Box 51
N-2007 Kjeller, NORWAY

Dr. George H. Rothe
Chief, Research Division
Geophysics Directorate
Headquarters Air Force Technical
Applications Center
Patrick AFB, Florida 32925-6001

Dr. Alan S. Ryall, Jr.
Center for Seismic Studies
1300 North 17th Street
Suite 1450
Arlington, VA 22209-2308

Dr. Jeffrey L. Stevens
S-CUBED,
A Division of Maxwell Laboratory
P.O. Box 1620
La Jolla, CA 92038-1620

Dr. Lawrence Turnbull
OSWR/NED
Central Intelligence Agency
CIA, Room 5G48
Washington, DC 20505

Professor Steven Grand
Department of Geology
245 Natural History Bldg
1301 West Green Street
Urbana, IL 61801

DARPA/PM
1400 Wilson Boulevard
Arlington, VA 22209

U.S. Geological Survey
ATTN: Dr. T. Hanks
National Earthquake Research Center
345 Middlefield Road
Menlo Park, CA 94025

Defense Technical Information Center
Cameron Station
Alexandria, VA 22314 (12 copies)

SRI International
333 Ravensworth Avenue
Menlo Park, CA 94025

Defense Intelligence Agency
Directorate for Scientific and
Technical Intelligence
Washington, D.C. 20301

Center for Seismic Studies
ATTN: Dr. C. Romney
1300 North 17th Street
Suite 1450
Arlington, VA 22209 (3 copies)

Defense Nuclear Agency
Shock Physics Directorate/SS
Washington, D.C. 20305

Dr. Robert Blandford
DARPA/GSD
1400 Wilson Boulevard
Arlington, VA 22209-2308

Defense Nuclear Agency/SPSS
ATTN: Dr. Michael Shore
6801 Telegraph Road
Alexandria, VA 22310

Ms. Ann Kerr
DARPA/GSD
1400 Wilson Boulevard
Arlington, VA 22209-2308

AFOSR/NPC
ATTN: Director
Bldg 410, Room C222
Bolling AFB, Washington, D.C. 20332

Dr. Ralph Alewine III
DARPA/GSD
1400 Wilson Boulevard
Arlington, VA 22209-2308

AFTAC/CA (STINFO)
Patrick AFB, FL 32925-6001

Mr. Edward Giller
Pacific Sierra Research Corp.
1401 Wilson Boulevard
Arlington, VA 22209

AFWL/NTESC
Kirtland AFB, NM 87171

Science Horizons, Inc.
Attn: Dr. Bernard Minster
Dr. Theodore Cherry
710 Encinitas Blvd., Suite 101
Encinitas, CA 92024 (2 copies)

U.S. Arms Control & Disarmament Agency
ATTN: Mrs. M. Hoinkes
Div. of Multilateral Affairs, Rm 5499
Washington, D.C. 20451

Dr. Jack Evernden
USGS - Earthquake Studies
345 Middlefield Road
Menlo Park, CA 94025

Dr. Lawrence Braile
Department of Geosciences
Purdue University
West Lafayette, IN 47907

Dr. G.A. Bollinger
Department of Geological Sciences
Virginia Polytechnical Institute
21044 Derring Hall
Blacksburg, VA 24061

Dr. L. Sykes
Lamont Doherty Geological Observatory
Columbia University
Palisades, NY 10964

Dr. S.W. Smith
Geophysics Program
University of Washington
Seattle, WA 98195

Dr. L. Timothy Long
School of Geophysical Sciences
Georgia Institute of Technology
Atlanta, GA 30332

Dr. N. Biswas
Geophysical Institute
University of Alaska
Fairbanks, AK 99701

Dr. Freeman Gilbert
Institute of Geophysics &
Planetary Physics
Univ. of California at San Diego
P.O. Box 109
La Jolla, CA 92037

Dr. Pradeep Talwani
Department of Geological Sciences
University of South Carolina
Columbia, SC 29208

University of Hawaii
Institute of Geophysics
Attn: Dr. Daniel Walker
Honolulu, HI 96822

Dr. Donald Forsyth
Department of Geological Sciences
Brown University
Providence, RI 02912

Dr. Jack Oliver
Department of Geology
Cornell University
Ithaca, NY 14850

Dr. Muawia Barazangi
Geological Sciences
Cornell University
Ithaca, NY 14853

Rondout Associates
Attn: Dr. George Sutton
Dr. Jerry Carter
Dr. Paul Pomeroy
P.O. Box 224
Stone Ridge, NY 12484 (3 copies)

Dr. M. Sorrells
Geotech/Teledyne
P.O. Box 28277
Dallas, TX 75228

Dr. Bob Smith
Department of Geophysics
University of Utah
1400 East 2nd South
Salt Lake City, UT 84112

Dr. Anthony Gangi
Texas A&M University
Department of Geophysics
College Station, TX 77843

Dr. Gregory B. Young
ENSCO, Inc.
5400 Port Royal Road
Springfield, CA 22151

Dr. Ben Menaheim
Weizman Institute of Science
Rehovot, ISRAEL 951729

Weidlinger Associates
Attn: Dr. Gregory Wojcik
620 Hansen Way, Suite 100
Palo Alto, CA 94304

Dr. Leon Knopoff
University of California
Institute of Geophysics & Planetary
Physics
Los Angeles, CA 90024

Dr. Kenneth H. Olsen
Los Alamos Scientific Laboratory
Post Office Box 1663
Los Alamos, NM 87545

Prof. Jon F. Claerbout
Prof. Amos Nur
Dept. of Geophysics
Stanford University
Stanford, CA 94305 (2 copies)

AFGL/XO
Hanscom AFB, MA 01731-5000

Dr. Robert Burrige
Schlumberger-Doll Research Ctr.
Old Quarry Road
Ridgefield, CT 06877

AFGL/LW
Hanscom AFB, MA 01731-5000

Dr. Eduard Berg
Institute of Geophysics
University of Hawaii
Honolulu, HI 96822

AFGL/SULL
Research Library
Hanscom AFB, MA 01731-5000 (2 copies)

Secretary of the Air Force (SAFRD)
Washington, DC 20330

Dr. Robert Phinney
Dr. F.A. Dahlen
Dept. of Geological & Geophysical Sci.
Princeton University
Princeton, NJ 08540 (2 copies)

Office of the Secretary Defense
DDR & E
Washington, DC 20330

Dr. Kin-Yip Chun
Geophysics Division
Physics Department
University of Toronto
Ontario, CANADA M5S 1A7

HQ DNA
Attn: Technical Library
Washington, DC 20305

New England Research, Inc.
Attn: Dr. Randolph Martin III
P.O. Box 857
Norwich, VT 05055

Director, Technical Information
DARPA
1400 Wilson Blvd.
Arlington, VA 22209

Sandia National Laboratory
Attn: Dr. H.B. Durham
Albuquerque, NM 87185

Los Alamos Scientific Laboratory
Attn: Report Library
Post Office Box 1663
Los Alamos, NM 87544

Dr. Gary McCartor
Mission Research Corp.
735 State Street
P. O. Drawer 719
Santa Barbara, CA 93102

Dr. Thomas Weaver
Los Alamos Scientific Laboratory
Los Alamos, NM 87544

Dr. W. H. K. Lee
USGS
Office of Earthquakes, Volcanoes,
& Engineering
Branch of Seismology
345 Middlefield Rd
Menlo Park, CA 94025

Dr. Al Florence
SRI International
333 Ravenswood Avenue
Menlo Park, CA 94025-3493